The Surprising Chemistry of 6-Azidotetrazolo[5,1-*a*]phthalazine: What a Purported Natural Product Reveals about the Polymorphism of Explosives

Aaron Gabriel Nunez Avila,[†] Benoît Deschênes Simard,[†] Joseph E. Arnold,[‡] Mathieu Morency,[†] Daniel Chartrand,[†] Thierry Maris,[†] Gilles Berger,[§] Graeme M. Day,*[,‡] Stephen Hanessian,*[,†] and James D. Wuest*[,†]

[†]*Département de Chimie, Université de Montréal, Montréal, Québec H2V 0B3 Canada*

[‡]*School of Chemistry, University of Southampton, University Road, Southampton SO17 1BJ United Kingdom*

[§]*Microbiologie, Chimie bioorganique et macromoléculaire, Faculté de Pharmacie, Université libre de Bruxelles (ULB), Boulevard du Triomphe, 1050 Bruxelles Belgium*

*Authors to whom correspondence may be addressed

Email: *james.d.wuest@umontreal.ca, stephen.hanessian@umontreal.ca, g.m.day@soton.ac.uk*

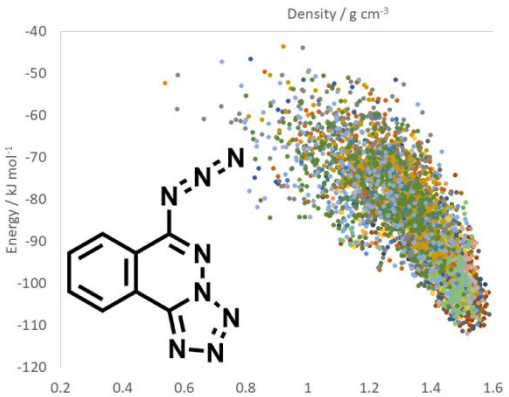

Abstract

6-Azidotetrazolo[5,1-*a*]phthalazine (ATPH) is a nitrogen-rich compound of surprisingly broad interest. It is purported to be a natural product, yet is closely related to substances developed as explosives and is highly polymorphic despite having a nearly planar structure with little flexibility. Seven solid forms of ATP have been characterized by single-crystal X-ray diffraction. The structures show diverse patterns of molecular organization, including both stacked sheets and herringbone packing. In all cases, N···N and C–H···N interactions play key roles in ensuring molecular cohesion. The high polymorphism of ATPH appears to arise in part from the ability of virtually every atom of nitrogen and hydrogen in the molecule to take part in close N···N and C–H···N contacts. As a result, adjacent molecules can adopt many different relative orientations that are energetically similar, thereby generating a polymorphic landscape with an unusually high density of potential structures. This landscape has been explored in detail by computational prediction of crystal structures. Studying ATPH has provided insights about the field of energetic materials, where access to multiple polymorphs can be used to improve performance and clarify how it depends on molecular packing. In addition, our work with ATPH shows how valuable insights about molecular crystallization, often gleaned from statistical analyses of structural databases, can also come from in-depth empirical and theoretical studies of single compounds that show distinctive behavior.

Introduction

Many natural products contain nitrogen, but few have nitrogen–nitrogen bonds.[1–5] The first structural characterization of a natural product with a nitrogen–nitrogen bond was reported in 1951,[6] when the toxic azoxyglycoside macrozamin (**1**) was described. The compound was initially extracted from seeds of the genus *Macrozamia*, a cycad plant widely distributed in tropical and subtropical parts of the world and long known to be toxic to humans and animals. Since 1951, more than 200 additional natural products with nitrogen–nitrogen bonds have been characterized, and many have other unusual structural features and noteworthy biological activity.

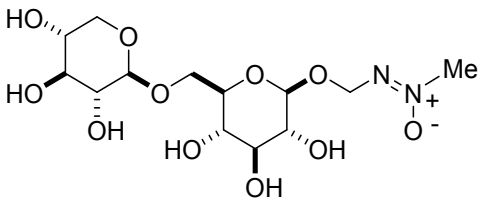

1 (Macrozamin)

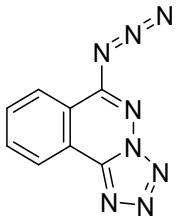

2 (ATPH)

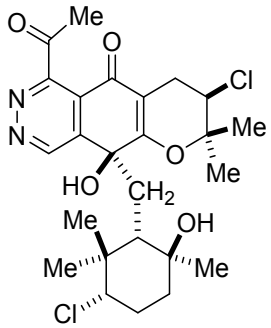

3 (Azamerone)

One of the most remarkable compounds included among natural products with nitrogen–nitrogen bonds is 6-azidotetrazolo[5,1-*a*]phthalazine (**2**; ATPH). ATPH was reported to have been extracted

from a culture of *Gymnodinium breve*,[7] a toxin-producing dinoflaggelate associated with red tides in the Gulf of Mexico. Even amidst the impressive structural diversity of natural products with nitrogen–nitrogen bonds, ATPH stands out as unusual. It contains an equal number of carbon and nitrogen atoms, and its six nitrogen–nitrogen bonds encompass an azido group, a tetrazole ring, and a phthalazine ring. The realm of natural products includes one other phthalazine, the meroterpenoid azamerone (**3**), which was isolated from cultures of a marine species of the bacterium *Streptomyces*.[8–10] However, the only azide or tetrazole reported to be a natural product is ATPH.

The structure of ATPH has been established by single-crystal X-ray diffraction.[7] Moreover, syntheses of ATPH by two different routes were described long before the compound was reported to be a natural product.[11,12] In the first method (Scheme 1), ATPH was prepared by the reaction of 1,4-dichlorophthalazine (**4**) with NaN_3.[11] In the second route, ATPH was made by the reaction of nitrous acid with dihydralazine, an antihypertensive agent that can be represented by structure **5** or its tautomers.[12] In either method of synthesis, ATPH presumably results from intramolecular azide-tetrazole isomerization of an intermediate azidophthalazine such as diazide **6**.[13,14] A second isomerization to give bis(tetrazole) **7** has not been reported to take place.

Scheme 1. Synthesis and Potential Isomers of ATPH

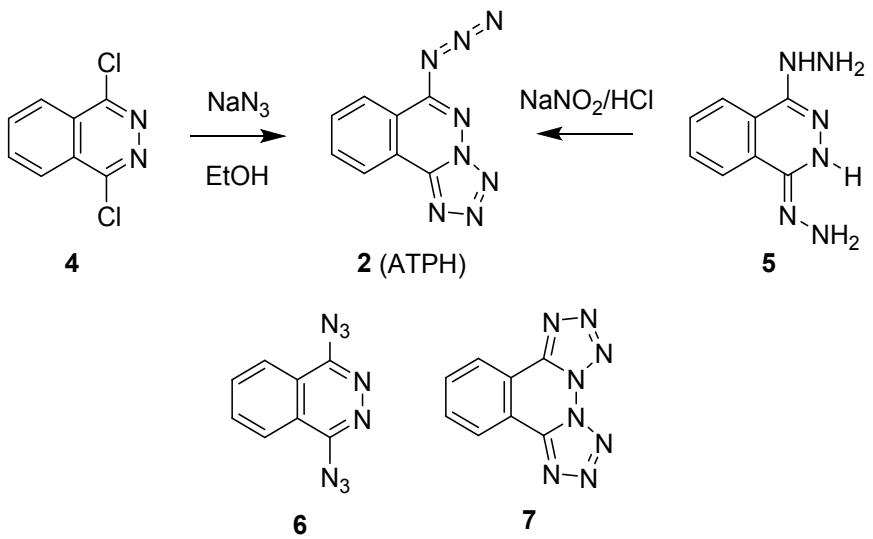

4 **2** (ATPH) **5**

6 **7**

Although the structure of ATPH is well established, it is so unusual that the status of the compound as a natural product remains in doubt. ATPH may be an artefact produced by culturing *Gymnodinium breve* in an artificial medium, and no studies of its purported biosynthesis have been reported. Nevertheless, the well-established existence of azamerone (**3**), along with recent advances in understanding how heteroatom-heteroatom bonds are created in nature,[15–17] offers support for classifying ATPH as a natural product. Intriguingly, the discovery that bacterial gene cassettes provide machinery for making hydrazines[2,18] and for carrying out biosynthetic diazotizations with nitrous acid[19] demonstrates that tools of the type used in laboratory syntheses of ATPH (Scheme 1) are also available to microorganisms.

Natural product or not, ATPH has many properties of interest, including a high level of ichthyotoxicity (LD_{100} = 0.4 μg mL^{-1})[7] and an apparent preference for asymmetric azidotetrazolo

structure **2** rather than for two plausible symmetric alternatives, diazide **6** or bis(tetrazole) **7**. Moreover, ATPH is an organic azide with a high N/C ratio and multiple nitrogen–nitrogen bonds, making the compound potentially explosive.[20,21] Indeed, ATPH is closely related to compounds being developed as lead-free primary explosives.[22,23]

ATPH has been found to have an additional property of significant interest, which is its ability to exist in multiple crystalline forms. This phenomenon, called polymorphism,[24] is commonplace in chemistry, but the high levels of polymorphism displayed by ATPH are very rare. In the Cambridge Structural Database (CSD), which has over 10^6 structures of small-molecule organic and organometallic compounds, fewer than 40% of the substances are polymorphic,[25] and a recent survey found that merely 13 compounds (0.0013%) are known to exist in five or more forms.[26] The most polymorphic compound in the CSD, named ROY for the red, orange, and yellow colors of its forms, has been studied for decades,[27] and 12 forms have now been structurally characterized by single-crystal X-ray diffraction.[28,29]

In the case of ATPH, one polymorph was known when we began our work.[7] We have now found six new forms, determined their structures by single-crystal X-ray diffraction, and compared the structures with those predicted to exist by computational methods. Analysis of the structures has provided broadly useful new insights about crystallization. In particular, our results highlight the importance of noncovalent N···N interactions in the structures of azides and show in detail how unusually high levels of polymorphism can arise, even in the case of compounds with nearly planar structures and limited conformational freedom.

Results and Discussion

Although no explosions involving ATPH occurred during our work, the compound decomposes vigorously when heated, with the evolution of copious volumes of black smoke. No more than about 5 g was ever prepared at one time, and precautions normally used in handling potentially explosive materials were taken whenever ATPH was manipulated in solid form. It is important to note that closely related compounds have been reported to become more explosive as their purity and the size of their crystals increase.[30]

Azide-Tetrazole Isomerization in ATPH. The preference of ATPH for an asymmetric azidotetrazolo structure was established by single-crystal X-ray diffraction,[7] and the report describing the initial synthesis included observations inconsistent with the formation of symmetric diazide **6** or bis(tetrazole) **7**.[11] However, the relative energies of azides and isomeric tetrazoles in solution are known to be affected by various factors, including substitution, temperature, and polarity of solvent.[13] Therefore, we began our study of ATPH by examining the accessibility of isomers **6** and **7**. After confirming that solutions of ATPH in DMSO-d_6 could be heated safely in the probe of an NMR spectrometer, we recorded variable-temperature ^{1}H NMR spectra. As the temperature was increased from 25 to 150 °C, we observed no broadening of the four aromatic signals characteristic of asymmetric structure **2** at δ 8.60 (d, ^3J = 8.1 Hz, 1H), 8.21 (dd, ^3J = 8.1 Hz, ^3J = 7.4 Hz, 1H), 8.19 (d, ^3J = 8.3 Hz, 1H), and 8.08 (dd, ^3J = 8.3 Hz, ^3J = 7.4 Hz, 1H).[13] This experiment established that azidotetrazolo structure **2** is favored in the range 25–150 °C, that

interconversion with symmetric isomers **6** or **7** is slow even at 150 °C, and that the barrier to isomerization is at least E_a = 21 kcal mol^{-1}.

Further insight was provided by using density functional theory (DFT) at the B3LYP/6-31+G(d,p) level to calculate the energies of azidotetrazole **2**, diazide **6**, and bis(tetrazole) **7**. At 298 K in the gas phase, asymmetric isomer **2** was estimated to be more stable than symmetric alternatives **6** and **7** by ΔG^o = 6.6 and 9.6 kcal mol^{-1}, respectively (Figure 1). Moreover, $\Delta G^‡$ for converting ATPH into diazide **6** was predicted to be 23.8 kcal mol^{-1}, and the corresponding barrier for transforming ATPH into bis(tetrazole) **7** was estimated to be 23.4 kcal mol^{-1}. These values are consistent with the results of our variable-temperature ^{1}H NMR studies. In addition, the calculations revealed that ATPH is expected to adopt an essentially planar conformation in which a nearly linear N_3 group is oriented as shown in structure **2** and Figure 1. Together, our experimental and computational studies confirm that ATPH favors an asymmetric azidotetrazolo structure under diverse conditions, contrary to suggestions in previous publications.[31,32]

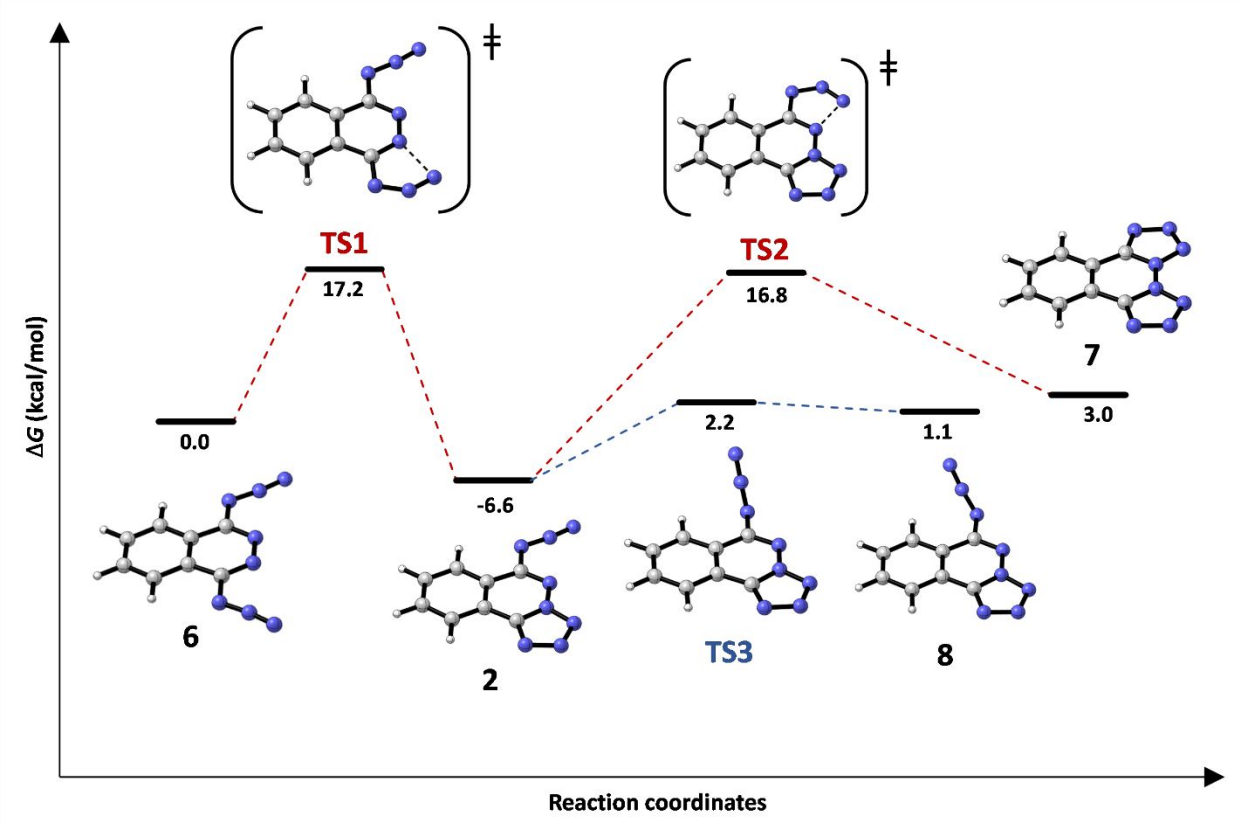

Figure 1. Computed energy profile (red dashes) showing ΔG^{o} (in kcal mol^{-1} at 298 K) for the gas-phase isomerization of ATPH (azidotetrazole **2**) to give symmetric diazide **6** and bis(tetrazole) **7**, with a second profile (blue dashes) corresponding to rotation around the C-N_3 bond of ATPH. TS1, TS2, and TS3 identify the transition states for the interconversions. All calculations used DFT at the B3LYP/6-31+G(d,p) level. Atoms of carbon appear in gray, hydrogen in white, and nitrogen in blue.

To understand why ATPH exists as azidotetrazolophthalazine **2** rather than as isomeric diazide **6** or bis(tetrazole) **7**, we compared electrostatic potentials in the three structures (Figure 2). Calculations show that electronic density is drawn from the azido groups to the adjacent heterocycles, most notably to the tetrazole rings. The push–pull arrangement of peripheral groups

in ATPH appears to be more stable than the push–push or pull–pull configurations in isomers **6** and **7**. Similar electronic interactions of azido groups with tetrazole rings have been observed in other azidotetrazoles.[22,33] This behavior is noteworthy because the tendency of energetic materials to explode on impact appears to increase as areas of strong positive potential become greater.[22,34] The initiation of many detonations is considered to be triggered by the cleavage of vulnerable bonds, such as the nitrogen–nitrogen bonds of azides and tetrazoles.[35] Charge redistributions of the type observed in ATPH are believed to weaken these triggering linkages and to increase sensitivity to impact.

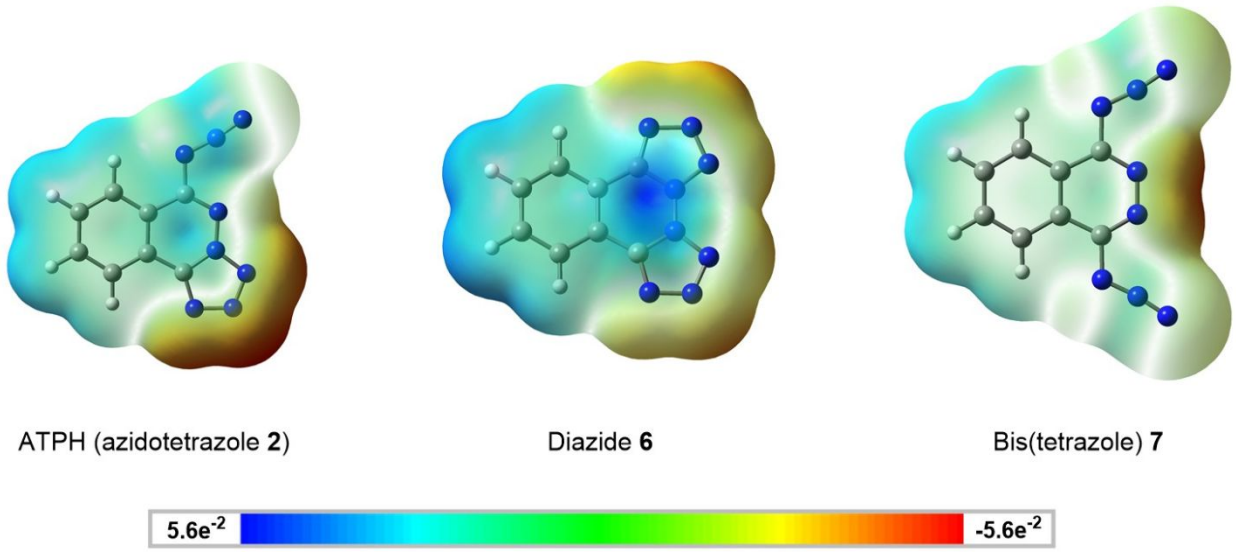

Figure 2. Surface electrostatic potentials of ATPH, diazide **6**, and bis(tetrazole) **7**. Atoms of carbon, hydrogen, and nitrogen appear in their standard colors. Electron densities were obtained by calculations at the B3LYP/6-31+G(d,p) level of theory, and the electrostatic potentials in atomic units were mapped on isodensities of 0.0004 e/Å^3.

Forms I and II of ATPH. In previous work,[7] nearly colorless needles grown by crystallizing ATPH from benzene were found to belong to the orthorhombic space group $P2_12_12_1$. The same form, which will be called Form I, can also be obtained by crystallizing ATPH from hot isopropanol. Cooling crystals of Form I to about 150 K induced their transformation into a new phase, Form II, which belongs to the monoclinic space group $P2_1$. The two structures are closely related and will be described together. ATPH adopts a virtually planar geometry in which the dihedral angle N–N–C–N between the azido group and the phthalazine ring ($|\theta_{azide}|$) is only 10.1° in Form I. Bond distances and angles for the azido group, tetrazole ring, and phthalazine ring are similar to those observed in related structures.[22,30,33,36–40] In particular, the N–N–N angle of the azido group is slightly bent (171.2° in Form I), as often observed in organic azides,[33] and N–N distances in the group (1.119 and 1.259 Å) have normal values. Other parameters are compiled in Table 1, and views of the structure of Form I are provided in Figure 3.

Table 1. Structural Data for Polymorphs of ATPH (**2**), as Determined by Single-Crystal X-Ray Diffraction, Along with Other Selected Properties

form	I[7]	II	III	IV	V	VI	VII
description	colorless needles	colorless needles	colorless needles	colorless plates	colorless prisms	colorless blocks	colorless blocks
crystal syst	orthorhombic	monoclinic	orthorhombic	monoclinic	monoclinic	monoclinic	monoclinic
space group	$P2_12_12_1$	$P2_1$	$Fdd2$	$P2_1/c$	$P2_1$	$P2_1/c$	$P2_1/c$
a (Å)	4.9738(2)	4.9733(1)	20.2505(10)	6.1658(1)	7.4796(2)	8.3082(4)	16.440(2)
b (Å)	12.2716(4)	12.1827(3)	33.1064(15)	17.1862(3)	5.1345(1)	13.8805(6)	17.2113(15)
c (Å)	14.6059(5)	14.5857(3)	5.3773(3)	8.8111(2)	11.9958(3)	8.0520(4)	14.4688(14)
α (deg)	90	90	90	90	90	90	90
β (deg)	90	92.319(1)	90	102.164(1)	104.155(1)	100.967(2)	116.005(5)
γ (deg)	90	90	90	90	90	90	90
V (Å^3)	891.49(6)	883.00(3)	3605.1(3)	912.72(3)	446.70(2)	911.61(7)	3679.5(7)

Z	4	4	16	4	2	4	16
Z'	1	2	1	1	1	1	4
ρ_{calc} (g · cm^{-3})	1.581	1.596	1.564	1.544	1.578	1.546	1.532
T (K)	150	100	100	100	100	100	100
R_1, $I > 2\sigma(I)$	0.0271	0.0329	0.0367	0.0429	0.0325	0.0315	0.0749
wR_2, $I > 2\sigma(I)$	0.0737	0.0949	0.0934	0.1094	0.0822	0.0893	0.2219
GoF	1.035	1.046	1.061	1.068	1.064	0.0344	0.820
organization	herringbone	herringbone	herringbone	sheet	herringbone	sheet	sheet
$\lvert\theta_{azide}\rvert$ (deg)[a]	10.1(2)	9.6(3)[d]	2.7(3)	2.10(15)	11.2(2)	2.03(14)	1.5(5)[d]
ν_{1400} (cm^{-1})[b]	1363, 1389	*c*	1360, 1388	1360, 1390	1367, 1386	1357, 1386	1363, 1389

[a]Dihedral angle N–N–C–N between the azido group and the phthalazine ring. [b]Specific position of the characteristic bands in the Raman spectrum near 1400 cm^{-1}. [c]Low-temperature phase not subjected to thermal or spectroscopic analysis. [d]Average value.

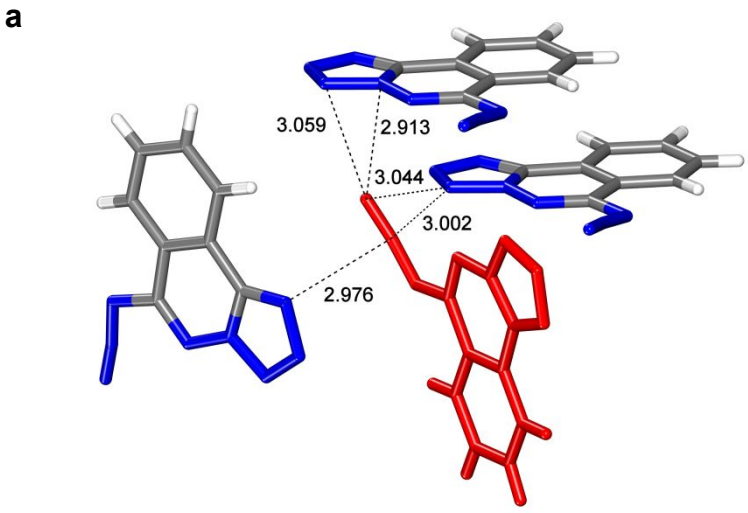

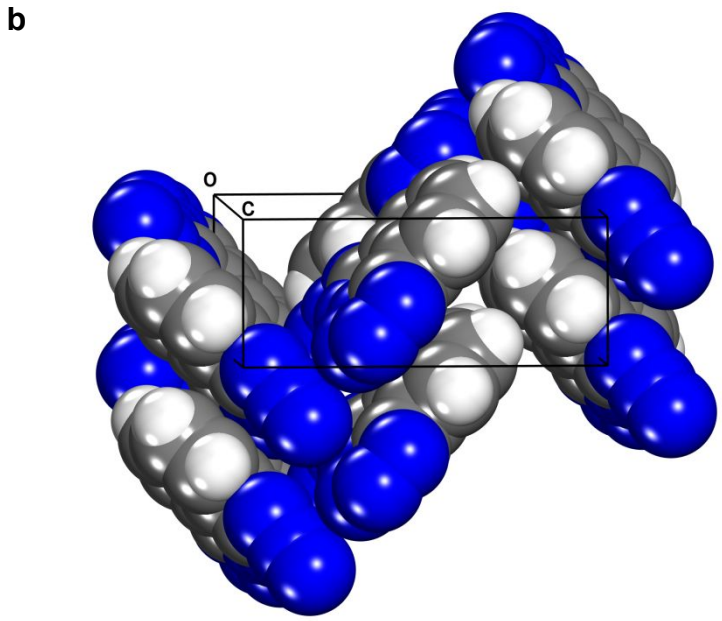

Figure 3. Representations of the structure of Form I of ATPH.[7] (a) Image showing a central molecule (red) and all intermolecular N···N interactions of its azido group that bring atoms of nitrogen closer together than the sum of their van der Waals radii (3.10 Å). The interactions are indicated by broken lines, with interatomic distances given in Å. Other short contacts of the central molecule are omitted. (b) View of the structure along the *c*-axis showing the characteristic herringbone packing. Unless indicated otherwise, atoms appear in their standard colors.

In Form I of ATPH, each molecule interacts with six neighbors to form multiple contacts with interatomic distances shorter than the sum of the van der Waals radii. The close contacts include two C–H···N interactions per molecule (2.558 Å) and numerous side-on and end-on azide-tetrazole contacts with N···N distances in the range 2.913–3.059 Å (Figure 3a), which are all significantly shorter than twice the van der Waals radius of nitrogen (2 × 1.55 = 3.10 Å). Short N···N contacts in the structure of Form I of ATPH were not noted by Hossain et al.,[7] who stated

that "…the crystal structure is stabilized by van der Waals interactions only." Significant N···N contacts are present in the structures of other azides,[30,33,36–38] but the potential of these interactions to control molecular organization in crystals has not yet been exploited systematically. This is surprising, given the long-standing interest in solid azides as explosives. In addition, the importance of azides in many other areas of science is growing rapidly,[41] as illustrated by their recent use in solid-state click reactions and in studies of the photodynamics of crystals.[42,43]

The presence of multiple short azide-tetrazole N···N contacts in Form I and low-temperature Form II may reflect the characteristic polarization of ATPH (Figure 2a), which is expected to strengthen association by enhancing the electrophilic character of the azido group and the electron-rich nature of the tetrazole ring. Recent computational studies have confirmed that interactions of the type suggested by side-on structure **8** (where D is a suitable donor) can offer significant stabilization and help determine the conformations and associative preferences of organic azides.[44] The structures of Forms I and II of ATPH suggest that end-on interactions (**9**) may also play an important role. For geometric reasons, the presence of multiple N···N interactions in Forms I and II forces adjacent molecules of ATPH to lie in different planes, thereby favoring herringbone packing (Figure 3b). Herringbone patterns of molecular organization in energetic materials are noteworthy because they are often associated with enhanced sensitivity to impact.[45–48] In alternative layered solids, kinetic energy introduced by mechanical stimuli may be more readily dispersed by converting it into the sliding motion of adjacent sheets.

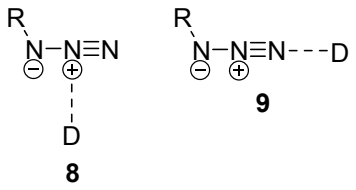

Screening for additional polymorphs of ATPH was facilitated by using confocal Raman microscopy to scan samples of crystals produced under various conditions. Bands near 1400 cm^{-1} proved to be particularly suitable for distinguishing solid forms, and DFT at the B3LYP/6-311+G(3df,2p) level was used to assign the bands to coupled modes involving the azido group, the phthalazine ring, and the tetrazole ring.[49] Positions of the bands in Form I and other polymorphs of ATPH are included in Table 1.

Form III of ATPH. Crystallization of ATPH induced by slow evaporation of solutions in isopropanol/acetone yielded nearly colorless needles of a new polymorph, Form III, in the orthorhombic space group *Fdd*2. As in Forms I and II, ATPH adopts an essentially planar structure, and the dihedral angle $|\theta_{azide}|$ defined by the azido group and the phthalazine ring is only 2.7°. The N–N–N angle of the azido group is again slightly bent (170.8°), and the N–N distances in the group (1.121 and 1.256 Å) are within their normal range. Table 1 summarizes additional data, and Figure 4 provides views of the structure.

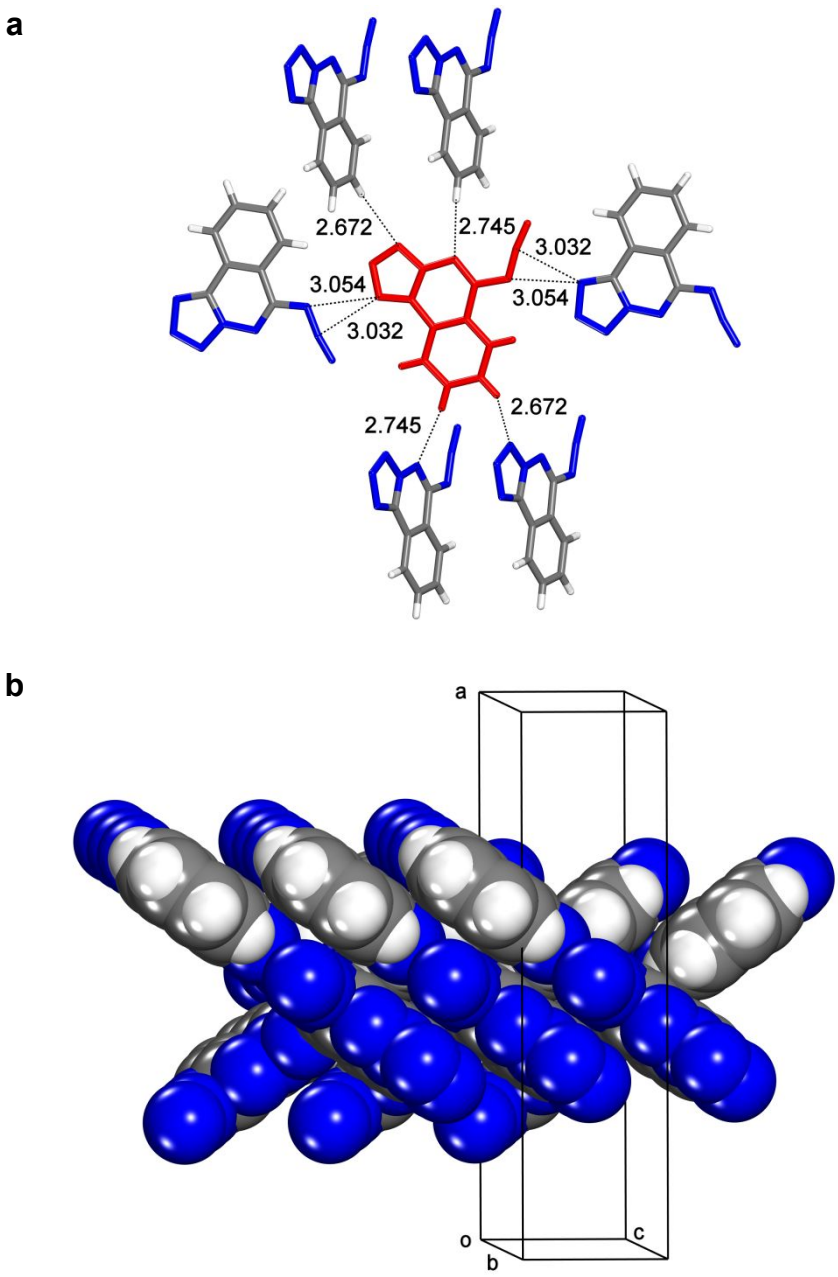

Figure 4. Representations of the structure of Form III of ATPH. (a) Image showing a central molecule (red), its six primary neighbors, and their key N···N and C–H···N interactions. All contacts that bring atoms closer together than the sum of their van der Waals radii are indicated by broken lines, with N···N and N···H distances given in Å. (b) View of the structure along the *b*-

axis showing the characteristic herringbone packing. Unless indicated otherwise, atoms appear in their standard colors.

In Form III, each molecule of ATPH interacts with six neighbors to establish eight intermolecular interactions that bring atoms closer together than the sum of their van der Waals radii (Figure 4a). Each azido group engages in a total of four N···N interactions with nearby tetrazole rings, with N···N distances (3.032 and 3.054 Å) that are shorter than the sum of the van der Waals radii (3.10 Å). Each molecule also forms four short C–H···N contacts (2.672 and 2.745 Å). As in Forms I and II, herringbone packing is observed (Figure 4b).

Form IV of ATPH. Colorless plates obtained when ATPH was crystallized by allowing a solution in EtOAc to evaporate slowly at 50 °C were found to correspond to a new polymorph, Form IV, which belongs to the monoclinic space group $P2_1/c$. As in Forms I–III, ATPH is virtually planar in Form IV, and the dihedral angle $|\theta_{azide}|$ is 2.1°. Values within the normal ranges are observed for the N–N–N angle of the azido group (171.4°) and its N–N distances (1.120 and 1.257 Å). Additional data are presented in Table 1, and a view of the structure is shown in Figure 5. Molecules of ATPH are joined head-to-tail to build tapes held together by short azide-tetrazole N···N contacts (2.995 and 3.088 Å) and by C–H···N interactions (2.631 Å). The tapes are connected by additional C–H···N interactions (2.622 Å) to produce sheets, which stack at a distance of 3.23 Å to give the observed structure.

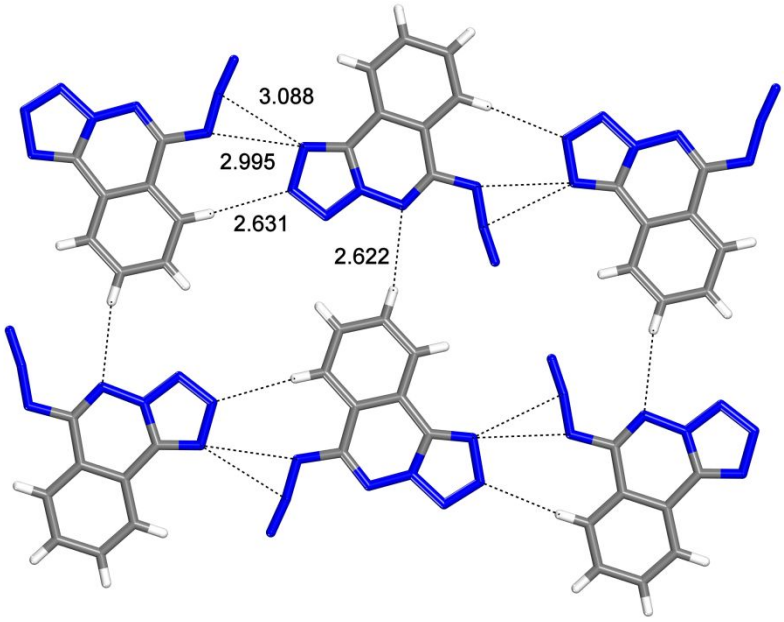

Figure 5. Representation of the structure of Form IV of ATPH, showing part of a sheet viewed approximately along the *ac*-diagonal. Atoms appear in their normal colors, and key contacts are indicated by broken lines, with N···N and N···H distances given in Å.

The discovery of Form IV of ATPH is significant because it shows that a compound related to established energetic materials can be induced to crystallize both in herringbone and layered arrangements. The widespread notion that explosives with layered molecular packing are inherently less sensitive to impact is based mainly on empirical comparisons of materials with different compositions, although the notion has also been supported by computational studies using a phonon up-pumping model.[50] ATPH shows that extensive polymorphic screening can be used in certain cases to produce energetic materials in either herringbone or layered forms, thereby allowing impact sensitivity and other parameters to be compared in cases where a single molecular component is arranged in distinctly different ways. Polymorphic screening is already widely used

to search for improved explosives,[24,51] but it typically serves as a way to adjust densities and velocities of detonation within a series of closely related structures. The behavior of ATPH suggests that new energetic materials can be devised to show distinctive polymorphic behavior, such as existing in large numbers of forms with diverse structural arrangements. In such cases, forms with lower impact sensitivity can be selected from among multiple candidates, and the relationship between explosive decomposition and molecular packing can be examined in detail.

Form V of ATPH. Crystals of new polymorph, Form V, were grown by layering hexane over solutions of ATPH in $CHCl_3$. Slow diffusion produced colorless prisms belonging to the monoclinic space group $P2_1$. As in previous cases, ATPH favors a nearly planar structure. The dihedral angle $|\theta_{azide}|$ involving the azido group is 11.2°, and the bond lengths lie within the normal ranges. Additional information is presented in Table 1, and views of the structure are shown in Figure 6. Each molecule takes part in four characteristic azide-tetrazole interactions (Figure 6a), with N···N distances (2.986 and 3.041 Å) shorter than the sum of the van der Waals radii (3.10 Å). In addition, each molecule engages in two short C–H···N interactions (2.631 Å). As in Forms I–III, the geometry of the N···N interactions forces neighboring molecules to lie in different planes, leading to herringbone packing (Figure 6b).

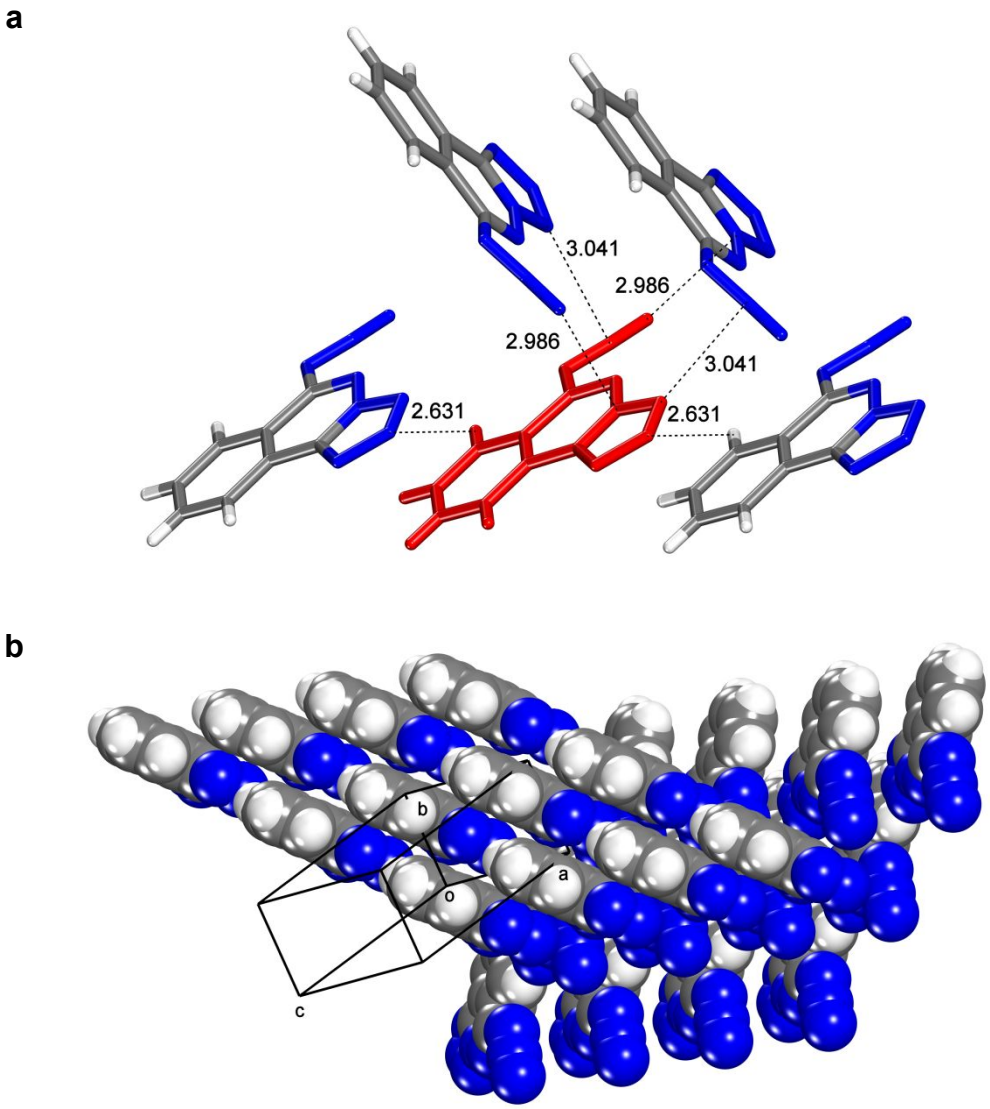

Figure 6. Representations of the structure of Form V of ATPH. (a) Image showing a central molecule (red), its four primary neighbors, and their close contacts. Key interactions are indicated by broken lines, with N···N and N···H distances given in Å. (b) View of the structure showing the characteristic herringbone packing. Unless indicated otherwise, atoms appear in their standard colors.

Form VI of ATPH. Although ATPH is sensitive to heat, we found that it melts without significant decomposition and recrystallizes as the melt is cooled. Screening the results of multiple melt crystallizations by polarized-light optical microscopy and Raman microscopy revealed that resolidified samples occasionally contain regions composed of new polymorph, Form VI. Monocrystalline areas could be cut away from surrounding material and used to solve the structure. In Form VI, which belongs to the monoclinic space group $P2_1/c$, ATPH is nearly planar and has normal bond lengths and a dihedral angle $|\theta_{azide}|$ of 2.0°. Table 1 summarizes additional data, and Figure 7 provides a view of the structure. Molecules of ATPH are joined head-to-tail along the *b*-axis to form tapes held together by short azide-tetrazole N···N contacts (3.081 Å). The tapes are connected by C–H···N interactions (2.527 and 2.569 Å) to produce sheets perpendicular to the *ac*-diagonal, and the sheets stack at a distance of 3.15 Å to give the observed structure.

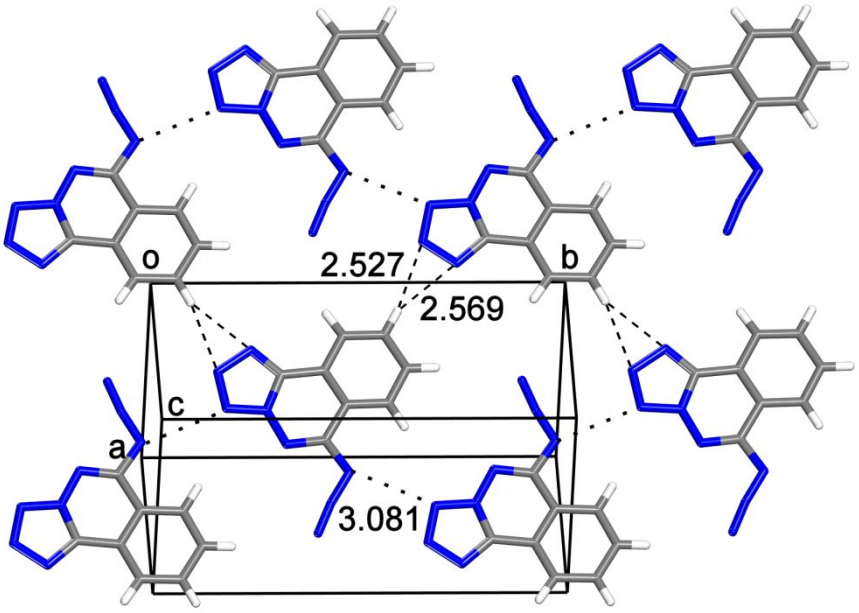

Figure 7. Representation of the structure of Form VI of ATPH, showing part of a sheet viewed along the *ac*-diagonal. Atoms appear in their standard colors, and key contacts are indicated by broken lines, with N···N and N···H distances given in Å.

Form VII of ATPH. In addition to yielding Forms I–VI with $Z' = 1$ or 2, crystallization of ATPH also gave rise to a new polymorph, Form VII, with $Z' = 4$. Form VII was produced as colorless blocks by allowing a solution of ATPH in 2-butanone/toluene to evaporate slowly at 50 °C, and it was found to belong to the monoclinic space group $P2_1/c$. As in all other structures examined, the azido group lies close to the plane of the phthalazine ring, and the average value of $|\theta_{azide}|$ is 1.5°. Table 1 summarizes additional data, and Figure 8 shows that multiple in-plane C–H···N interactions help lead to the formation of a structure composed of stacked sheets. Remarkably, the shortest intermolecular N···N distances within the sheets (about 3.18 Å) are significantly longer than twice the sum of the van der Waals radii (2 × 1.55 = 3.10 Å).

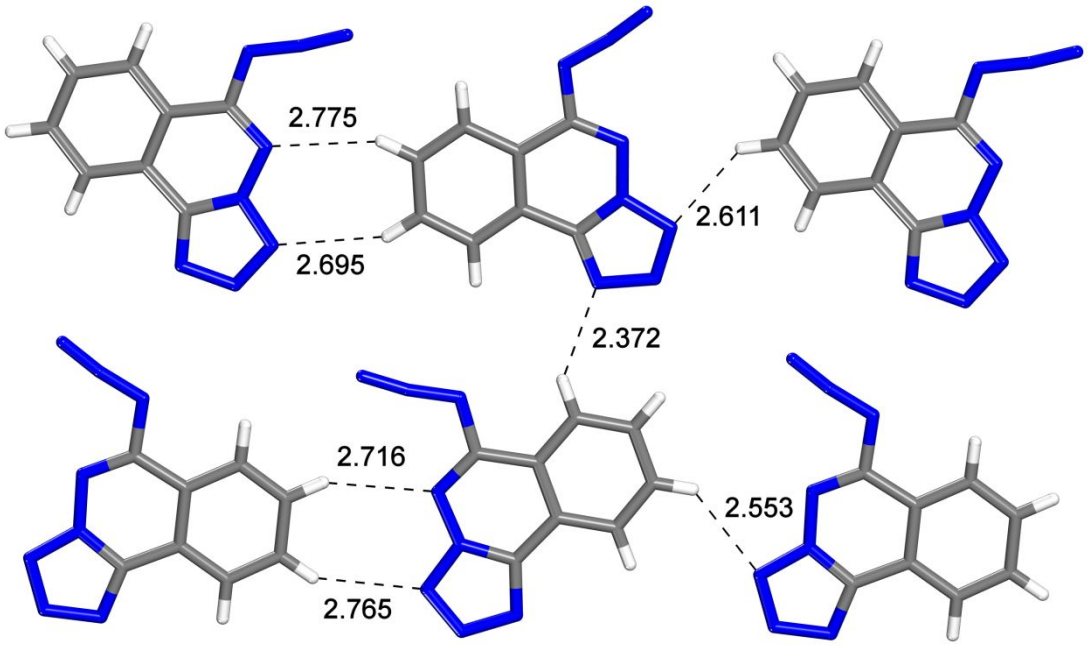

Figure 8. Representation of the structure of Form VII of ATPH, showing part of a sheet viewed along the *ac*-diagonal. Atoms appear in their standard colors, and key contacts are indicated by broken lines, with N···H distances given in Å.

We also found two related structures (Forms VIIa and VIIb) composed of stacked sheets like those of Form VII. Forms VIIa and VIIb were observed repeatedly in different samples. Their simulated powder X-ray diffraction patterns are closely related, and reconstructed precession patterns display characteristic diffuse scattering in the direction of stacking. These observations suggest that stacking is not commensurate, that the number of layers in a unit cell may vary or be modulated, and that Forms VIIa and VIIb should be regarded as different versions of a single structure in which ATPH forms stacked sheets.[49]

Origins of the High Polymorphism of ATPH. In general, polymorphs that can be isolated and characterized vary little in energy (≤ 1–2 kcal mol^{-1}),[24,52] and potential forms outside this range are usually inaccessible. Even so, other polymorphs often lie close in energy to the most stable form, and it has been suggested that all compounds can exist in different polymorphic forms and that the number of known forms reflects the effort made to find them.[53] Polymorphism is indeed common, yet few compounds have proven to resemble ROY, the current CSD record-holder,[27–29] by existing in many solid forms. The high polymorphism of ATPH is therefore noteworthy, especially because the seven known forms have resulted from routine screening.

ATPH adopts a conformation that is essentially the same in all known structures, so the conspicuous polymorphism of the compound does not arise from high molecular flexibility. Moreover, statistical analyses of the CSD have not shown that polymorphism and flexibility are closely correlated.[25,54,55] To probe the unusual behavior of ATPH, we constructed Hirshfeld surfaces and related two-dimensional fingerprint plots corresponding to molecules in selected polymorphs.[56,57] For simplicity, only forms with $Z' = 1$ were analyzed. The Hirshfeld surface of a molecule in a crystal traces the origin of local electron density, usually by showing where the density contributed by atoms in the molecule is equal to the density derived from all other atoms in the structure. The surface can be colored to reflect parameters indicating close intermolecular contacts, such as the distance from the surface to the nearest atomic nucleus in another molecule. Related fingerprint plots can be used to show the relative number of points on the Hirshfeld surface that have specific values of distance to the nearest external atomic nucleus (d_e) and distance to the nearest internal atomic nucleus (d_i). As the frequency of finding a particular coordinate (d_e, d_i) increases, the color at that point on the fingerprint plot changes from blue to red.

Figure 9 shows how various interatomic contacts contribute to the Hirshfeld surfaces of molecules of ATPH in the five polymorphs with $Z' = 1$ (Forms I, III, IV, V, and VI). Figure 10 presents the corresponding fingerprint plots, both unfiltered (to portray contacts involving all atoms in ATPH) and filtered (to focus attention on N···N and C–H···N contacts). Detailed structural analyses of Forms I–VI (Figures 3–7) establish that multiple short N···N and C–H···N contacts are present in all six structures. Figure 9 supports this assessment quantitatively by showing that N···N and C–H···N contacts together contribute 55–70% of the entire Hirshfeld surfaces corresponding to the five polymorphs with $Z' = 1$. The unfiltered plots in Figure 10 are generally similar because the structures are all composed of ATPH, and the conspicuous long spikes (d_e or $d_i \approx 1.0$ or 1.4) arise from C–H···N contacts, as confirmed by the corresponding filtered plots. Comparison of the filtered N···N plots reveals that Forms IV and VI have a significantly lower frequency of points near $d_e \approx d_i \approx 1.6$ Å arising from close N···N contacts. This observation is consistent with the finding that these two forms favor sheet structures in which N···N interactions are less important than in the herringbone arrangements of the other forms.

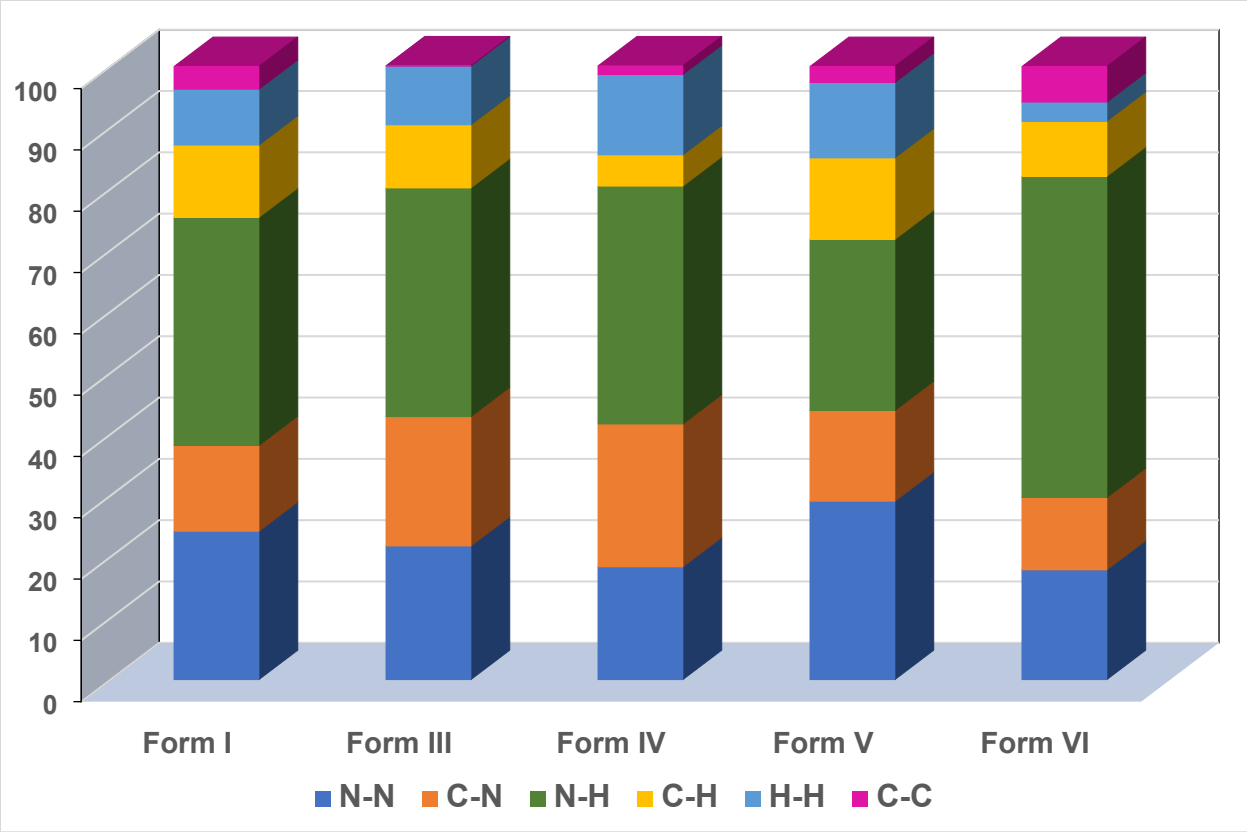

Figure 9. Percentage contributions made by various interactions to the Hirshfeld surfaces of molecules of ATPH in the five polymorphs with $Z' = 1$.

Form	Unfiltered (to show all contacts)	Filtered (to show reciprocal N···N contacts)	Filtered (to show reciprocal C–H···N contacts)
Form I	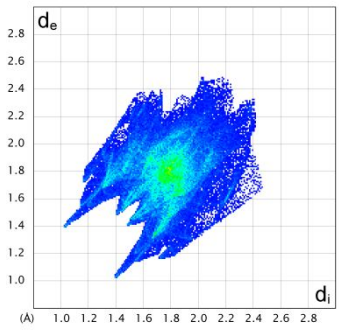	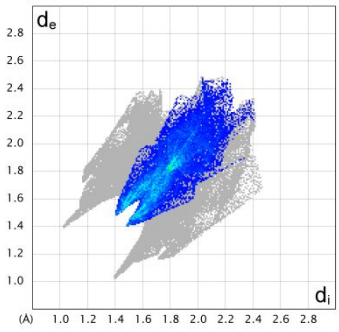	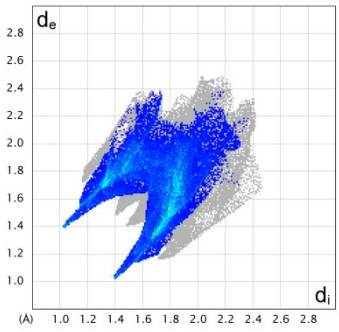

Form III	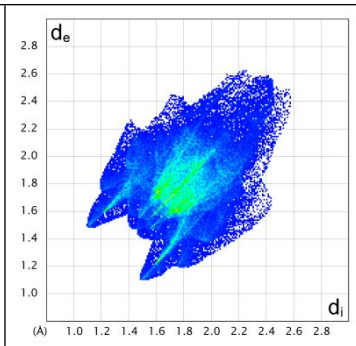	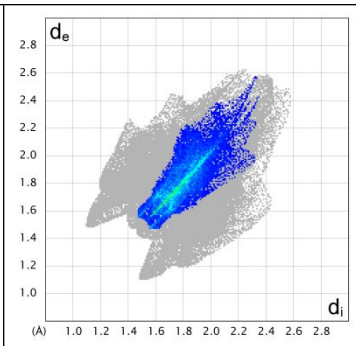	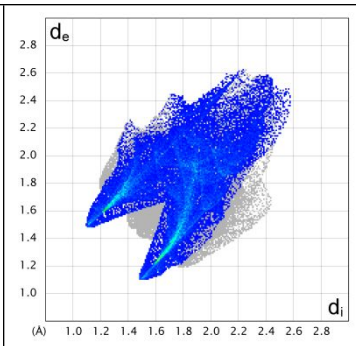
Form IV	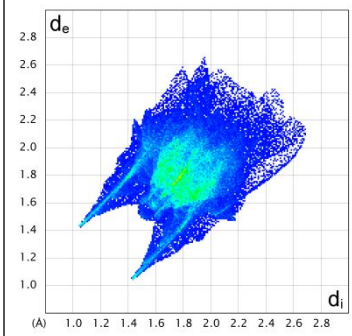	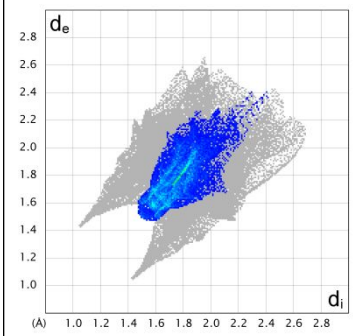	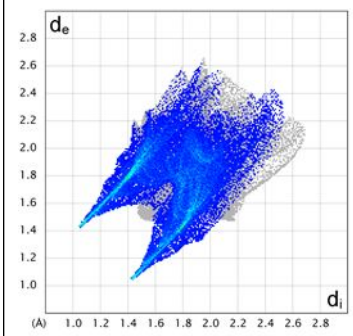
Form V	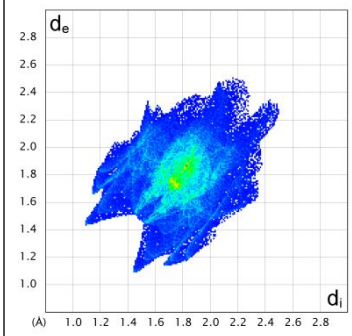	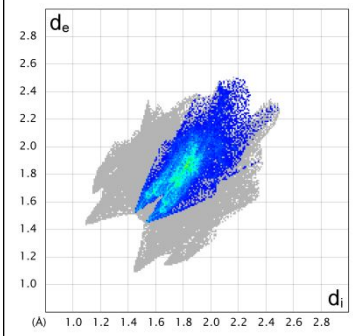	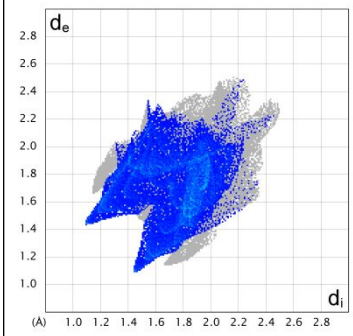
Form VI	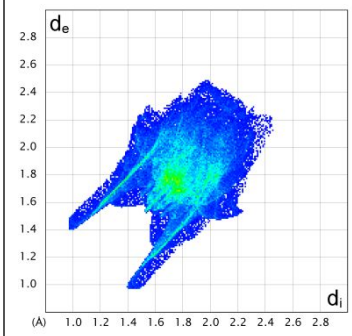	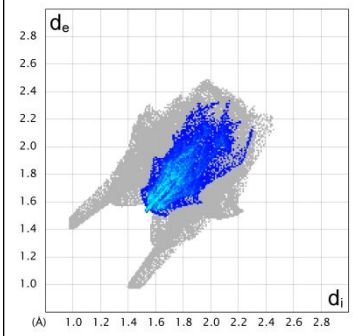	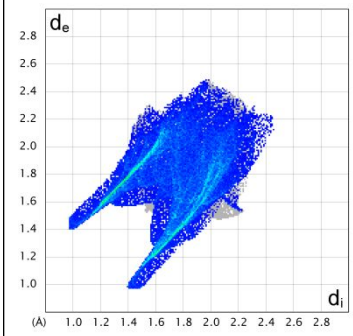

Figure 10. Two-dimensional unfiltered and filtered fingerprint plots of the Hirshfeld surfaces corresponding to molecules of ATPH in the five polymorphs with $Z' = 1$. The plots show the frequency of finding points on the surface with particular values of d_e and d_i (distances to the nearest external and internal atomic nuclei). The colors at each point range from blue to red as the frequency increases.

ATPH joins a select set of compounds in the CSD that exist primarily in a single conformation but are highly polymorphic.[58,59] Hidden among 10^6 inventoried structures, such compounds can easily be overlooked; when they are noticed, it is tempting to dismiss them as oddities in the realm of molecular crystallization. In fact, their unusual behavior is a potentially valuable source of ideas about the origin of polymorphic diversity. Unfortunately, factors underlying the properties of these special compounds cannot be identified by statistical analyses of the CSD, because the set of examples is too small. Instead, their behavior must be examined in other ways, such as by carefully analyzing observed and predicted structures.

Inspection of the seven fully characterized structures of ATPH reveals the predominance of N···N and C–H···N interactions, as measured by their collective contribution to Hirshfeld surfaces (Figure 9) and by the presence of multiple N···N and C–H···N contacts with distances shorter than the sum of the van der Waals radii of the atoms involved (Figures 3–7). These contacts are generally weaker and less directional than interactions such as hydrogen bonds, which can play major roles in controlling molecular organization in solids. Even so, the cohesion of molecules of ATPH may be strong enough to keep metastable structures that are formed during initial stages of crystallization from rearranging to favor the emergence of more stable forms. Moreover, Figures

3–7 show that virtually every atom of nitrogen and hydrogen in ATPH takes part in close N···N and C–H···N contacts in at least one polymorph. As a result, each molecule of ATPH and its closest neighbors can adopt many relative orientations, yet still allow the resulting structure to incorporate enough N···N and C–H···N contacts to ensure stability.

Crystal Structure Prediction (CSP) of ATPH. To confirm the origins of the high polymorphism of ATPH and to identify accessible forms that might remain undiscovered, we undertook CSP using a global search for local minima on the lattice-energy surface.[60] The initial CSP approach employed quasi-random structure generation, followed by energy minimization using an empirically-parameterized repulsion-dispersion method with atomic multipole electrostatics.[61,62] At this stage, the molecular geometry of ATPH was held fixed in the DFT-optimized planar conformation of the isolated molecule, as represented by structure **2** in Figure 1. As a result, this preliminary assessment did not consider potential polymorphism resulting from isomerism or from alternative conformations generated by changing the dihedral angle $|\theta_{azide}|$ substantially. These modifications were deemed unlikely to yield low-energy crystal structures because of their high molecular energies. The landscape of potential polymorphs was explored for structures in the 25 most frequently observed space groups ($P2_1/c$, $P2_12_12_1$, $P\bar{1}$, $P2_1$, $Pbca$, $C2/c$, $Pna2_1$, Cc, $Pca2_1$, $C2$, $P1$, $Pbcn$, Pc, $P2_12_12$, $Fdd2$, $Pccn$, $P2/c$, $I4_1/a$, $R\bar{3}$, $P4_1$, $P4_32_12$, $P4_12_12$, $P4_3$, $P3_2$, and $P3_1$) with one molecule in the asymmetric unit ($Z' = 1$), as well as in the 5 most frequently observed space groups with $Z' = 2$ ($P\bar{1}$, $P2_1/c$, $P2_1$, $P2_12_12_1$, and $P1$).

The predicted polymorphic landscape is densely populated (Figure 11a), with 12 structures lying within 0.5 kcal mol^{-1} of the global minimum and 228 within 1.7 kcal mol^{-1}, which is the range of

energies that includes 95% of all known polymorphs.[52] The large number of possible structures supports the conclusion that ATPH is unusually predisposed to polymorphism, and the diversity of packing arrangements within the predicted structures demonstrates that neighboring molecules can engage in N···N and C–H···N contacts in many different ways without changing the lattice energy substantially.

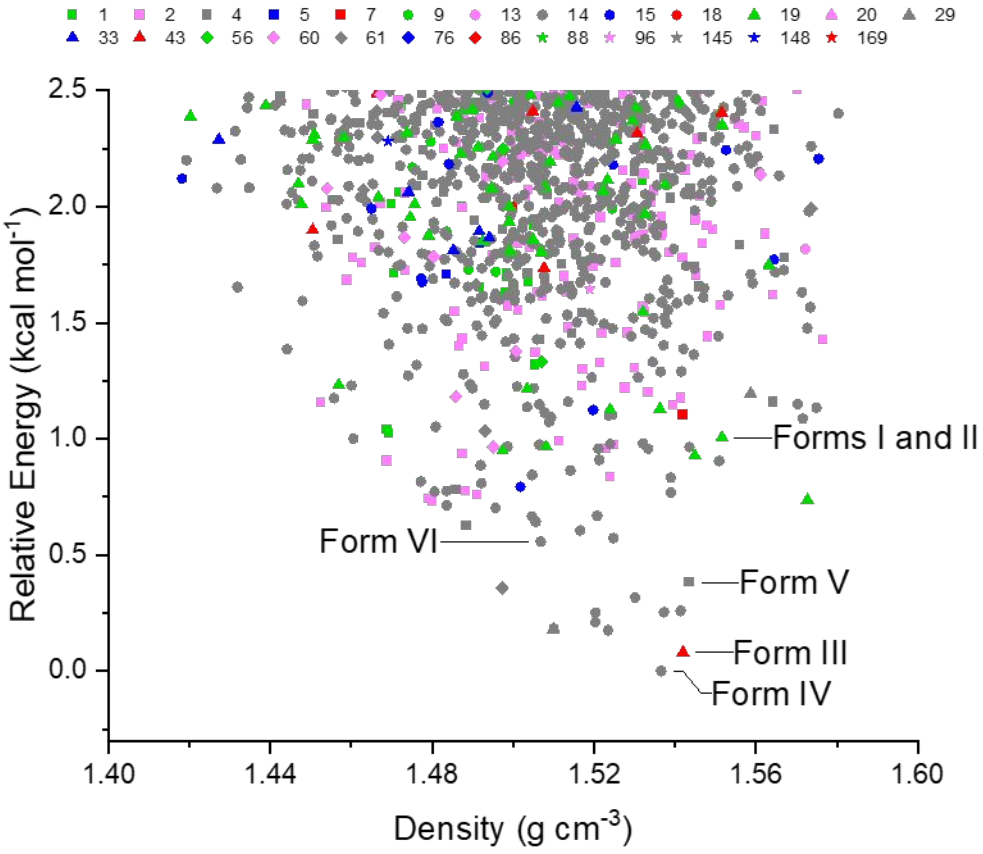

a

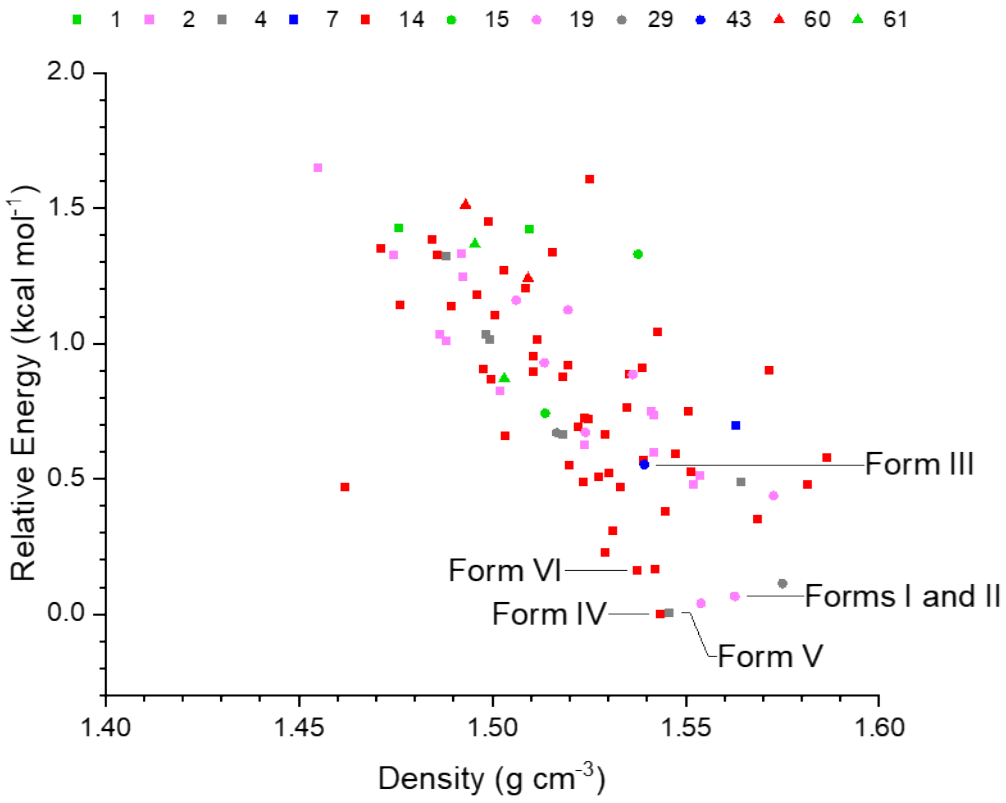

b

Figure 11. (a) Plot showing the energies and densities of crystal structures of ATPH as predicted using an empirically parametrized force field with atomic multipole electrostatics. The polymorphic landscape was explored for structures with $Z' = 1$ in the 25 most frequently observed space groups, and with $Z' = 2$ in the 5 most frequently observed space groups. ATPH was held in its optimized planar gas-phase conformation. Each plotted point represents a predicted polymorph, and the color identifies the space group according to the legend. (b) Analogous plot after re-optimization at the periodic DFT-D level of theory. The structures that were optimized were taken from the 1.195 kcal mol^{-1} low-energy window of the initial CSP. Structures corresponding to the observed Forms I, II, III, IV, V, and VI are labeled.

The predicted crystal structures of lowest energy are provided in the Supporting Information. Five characterized polymorphs of ATPH have $Z' = 1$ (Forms I, III, IV, V, and VI), and all of them appear within the set of structures predicted to have the lowest energies at the force-field level. The global energy minimum and the structure predicted to have the second lowest energy correspond to experimental Forms IV and III, respectively (Figure 11a). Forms V, VI, and I (in order of decreasing calculated stability) were found at slightly higher energies, all within just over 1 kcal mol^{-1} of the global energy minimum (Figure 11a). Energy minimization of Form I ($Z' = 1$) and the related low-temperature Form II ($Z' = 2$) proved to give the same structure. How well these matches fit the observed structural data was assessed by determining the root-mean-square deviation (RMSD) in atomic positions within a cluster of 30 molecules taken from the predicted and experimental crystal structures, as calculated using the COMPACK algorithm.[63] $RMSD_{30}$ values for structures predicted at the force-field level are shown in Table 2.

Table 2. $RMSD_{30}$ Values and Energies (Relative to the Global Minimum) for Predicted Matches to the Experimentally Observed Polymorphs of ATPH[a]

polymorph	force field		periodic DFT-D	
	$RMSD_{30}$ (Å)	relative energy (kcal mol^{-1})	$RMSD_{30}$ (Å)	relative energy (kcal mol^{-1})
Form I	0.16	1.006	0.13	0.066
Form II	0.24	1.006	0.22	0.066
Form III	0.68	0.079	0.66	0.552

Form IV	0.27	0	0.26	0
Form V	0.61	0.382	0.58	0.004
Form VI	0.21	0.557	0.18	0.162

[a]Results shown after the force-field and periodic DFT-D stages of optimization

Using DFT-D to Re-optimize the Predicted Crystal Structures of ATPH. In performing CSP on ATPH, we found that the relative energies of predicted structures were very sensitive to the level of theory used to describe the intermolecular electrostatic interactions, as described in greater detail in the Supporting Information. In addition, energetic errors arising from fixing ATPH in its optimized planar gas-phase conformation are also potentially important, given that $|\theta_{azide}|$ varies by about 11° in the polymorphs characterized experimentally. To increase our confidence in the calculated relative energies, we re-optimized the 86 predicted structures of lowest energy (those within 1.195 kcal mol^{-1} of the global minimum) to allow the molecular geometry of ATPH to adapt within each crystal structure. The re-optimization used periodic DFT calculations with the PBE functional and the D3 empirical dispersion correction as implemented in VASP.[64,65]

In the resulting distribution of structures (Figure 11b), all six matches to the experimental polymorphs proved to lie within 0.60 kcal mol^{-1} of the global minimum. After re-optimization (DFT-D), the predicted structure corresponding to Form IV remained the global energy minimum. However, the new calculated energy difference between Form IV ($|\theta_{azide}|$ = 2.1° as determined experimentally) and Form V ($|\theta_{azide}|$ = 11.2°) was found to be only 0.004 kcal mol^{-1}. Despite having completely different sets of intermolecular interactions, Forms IV and V are predicted to be energetically equivalent within computational error. Clearly, Form V was disfavored in initial calculations at the force-field level by constraining ATPH to have θ_{azide} = 0. As shown in Table 2,

geometric agreement between predicted and observed crystal structures was improved for all polymorphs by DFT-D re-optimization. Although our polymorphic screening was carried out using only routine methods without automation, it was effective enough to have produced four of the six $Z' = 1$ and $Z' = 2$ structures predicted to be the most stable.

Experimental Determination of the Relative Stabilities of the Observed Polymorphs of ATPH. Phase-pure samples of polymorphs of ATPH could be prepared under well-defined conditions of crystallization, as described in the Experimental Section. Phase purity was assessed by examining the region near 1400 cm^{-1} in Raman spectra and by comparing powder X-ray diffraction patterns of the bulk samples with simulated patterns derived from structures determined by single-crystal X-ray diffraction. The production of phase-pure samples allowed us to examine various properties of the polymorphs, including their relative stability. For all five $Z' = 1$ forms, data obtained by differential scanning calorimetry (DSC) are summarized in Figure 12. All samples showed similar melting behavior, with an onset near 150 °C and a peak near 152 °C. With the exception of Form V, all samples showed subtle transitions in the range 136–145 °C characterized by a small endotherm followed by a small exotherm. Raman spectroscopy and variable-temperature powder X-ray diffraction were used to determine that the transitions near 140 °C correspond to the conversion of Forms I, III, IV, and VI into Form V. The illustrative series of variable-temperature powder X-ray diffraction patterns in Figure 13 shows the transformation of Form III into Form V, and other series are provided in the Supporting Information.

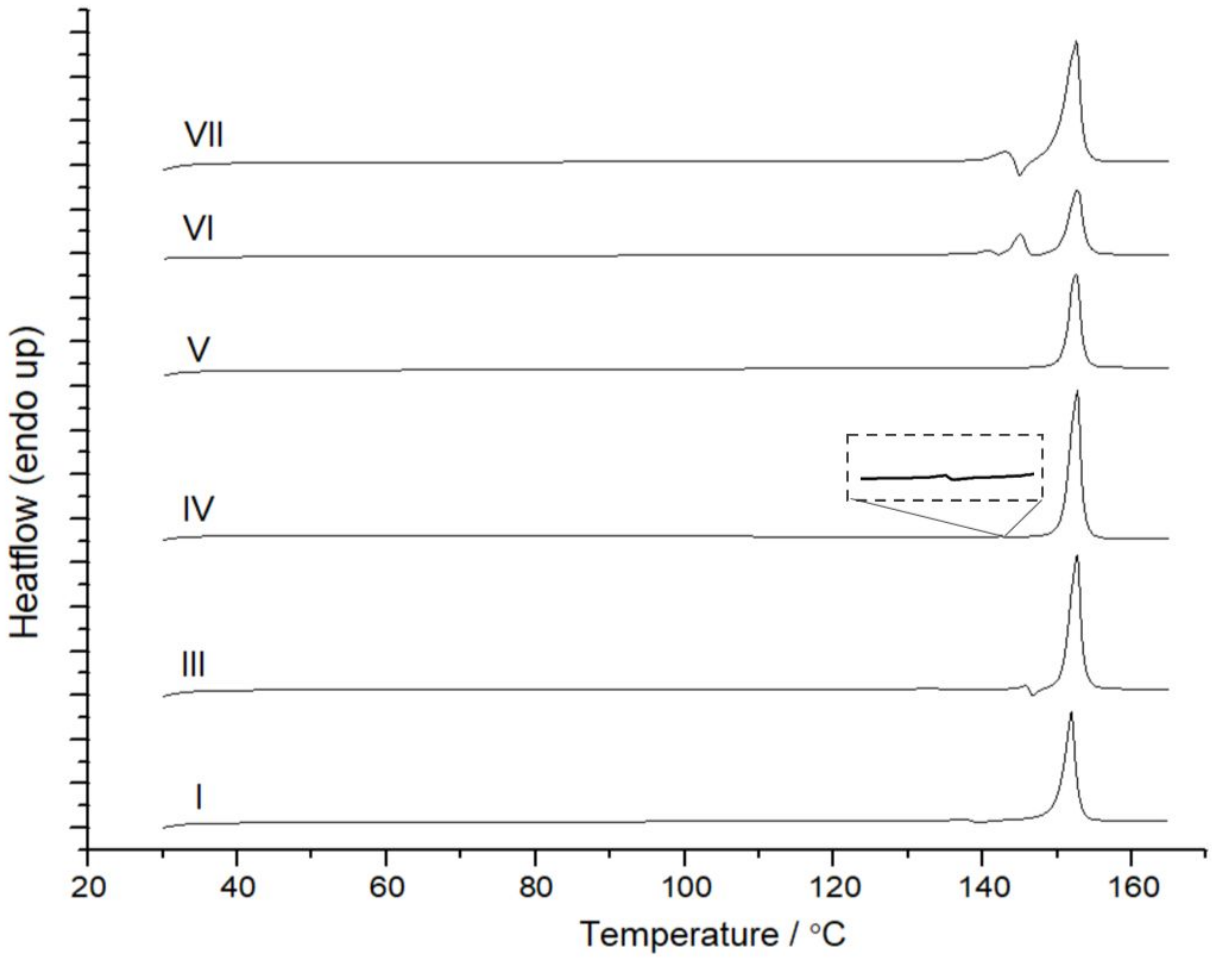

Figure 12. DSC curves corresponding to $Z' = 1$ Forms I, III, IV, V, and VI of ATPH. The heating rate was 20 °C/min, and aluminium pans used for the measurements were sealed manually to avoid pressure-induced polymorphic transformations. In the case of Form IV, an enlarged view of the region near 140 °C is provided to show the transition to Form V.

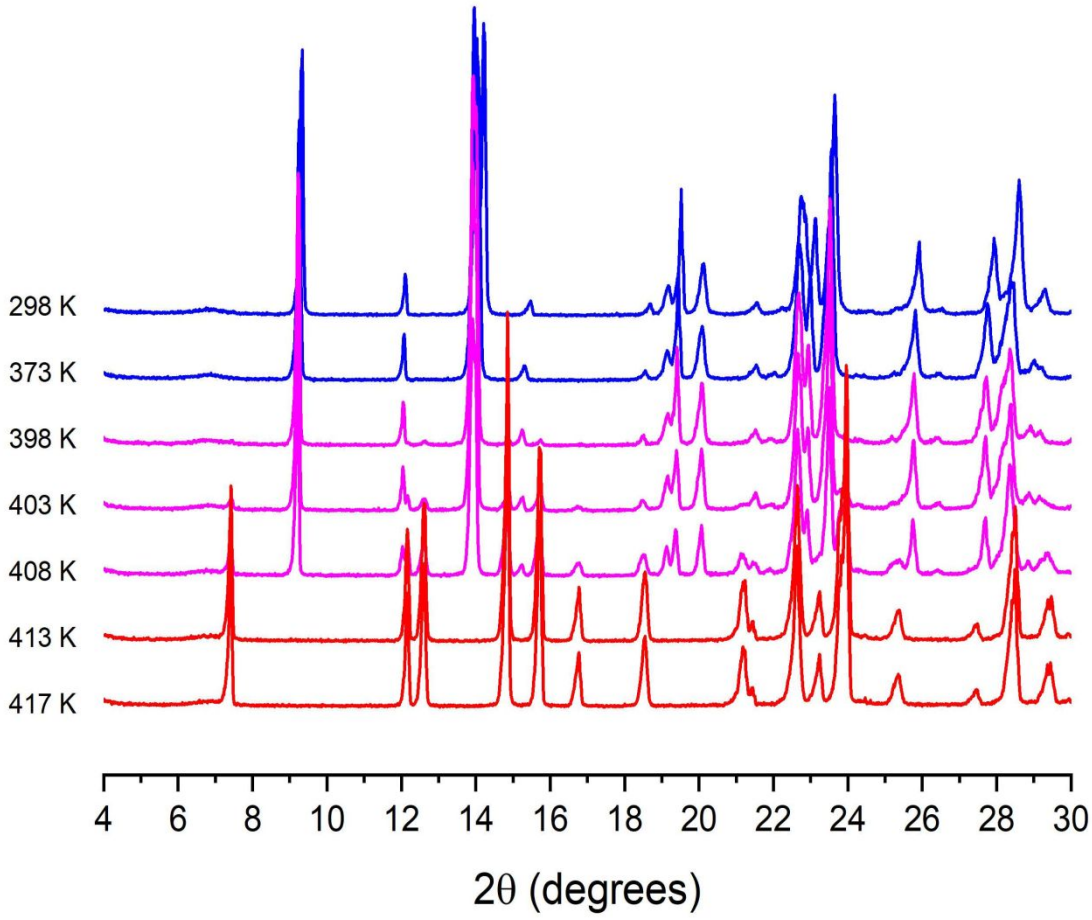

Figure 13. Representative variable-temperature powder X-ray diffraction patterns showing the thermal transformation of Form I of ATPH into Form V.

These experiments established that Form V is more stable than the other characterized $Z' = 1$ polymorphs at elevated temperatures. Additional information about relative stability was obtained by mixing phase-pure samples of the polymorphs with isopropanol, stirring the resulting slurries rapidly at 25 °C for extended periods, recovering the solids by filtration, and using powder X-ray diffraction and Raman spectroscopy to identify the forms recovered. Form VI could not be included in these studies because it needed to be extracted from limited areas of recrystallized melts, and sufficient material was not available. After 72 h of stirring in isopropanol at 25 °C,

Forms I, IV, and V remained unchanged, whereas Form III was converted into Form V, and Form VII was transformed into Form I. When the experiments were carried out at 50 °C for 24 h, all polymorphs examined except Form I were transformed into Form V. Further work revealed that Form I is more soluble than Form V at 25 °C, thereby showing that Form V is monotropically related to the other known polymorphs and is more stable at all temperatures. These findings agree well with the results of CSP after re-optimization using periodic DFT-D, which identified Form V (along with energetically equivalent Form IV) as the most stable structure on the polymorphic landscape. The order of stability determined by CSP for structures with $Z' = 1$ or $Z' = 2$ is V ≈ IV > I = II > VI > III.

Potential Undiscovered Polymorphs of ATPH. Of the six crystal structures of ATPH predicted to have the lowest energies, four correspond to known polymorphs. Only Form III sits outside this group, with a calculated energy only 0.55 kcal mol^{-1} above Forms IV and V. These results make us confident that the calculated energies are reliable and that other structures predicted to have low energies are potential undiscovered polymorphs of ATPH. The large number of such low-energy structures suggests that more polymorphs of ATPH can be isolated.

In particular, we highlight the two as-yet unobserved forms that lie among the six structures predicted to have the lowest energies. Between Forms V and I in energy is a predicted structure belonging to space group $P2_12_12_1$ with $Z' = 2$. Molecules of ATPH in this structure are packed in a herringbone pattern similar to the one observed in Forms I and II, but with a change in relative molecular orientations. The structure of Form I (as predicted by DFT-D) and the currently unobserved $P2_12_12_1$ structure are overlayed in Figure 14a. Between Forms I and VI in energy is a

predicted structure belonging to space group $Pca2_1$, which incorporates tapes held together by short azide–tetrazole N···N contacts, as seen in Form VI. The tapes form sheets in Form VI, but they are packed in a herringbone manner in the undiscovered $Pca2_1$ structure, with short C–H···N (tetrazole) interactions between tapes (Figure 14b). The high latent polymorphic potential of ATPH makes the compound an attractive subject for testing new ways to increase the diversity of accessible solid forms. The missing low-energy $P2_12_12_1$ and $Pca2_1$ structures are conspicuous targets for polymorphic screening.

a

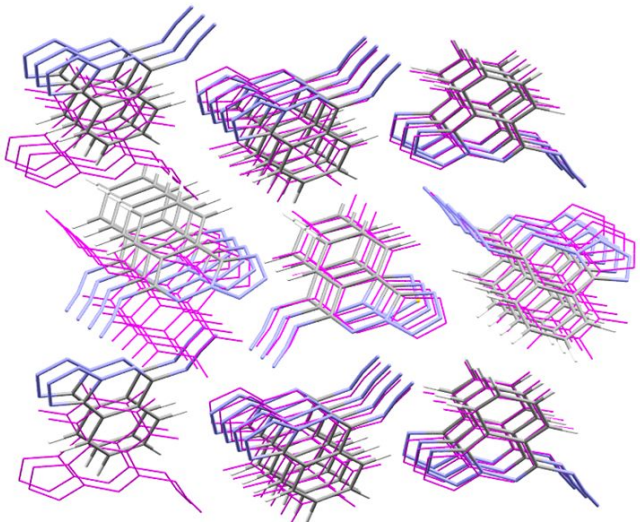

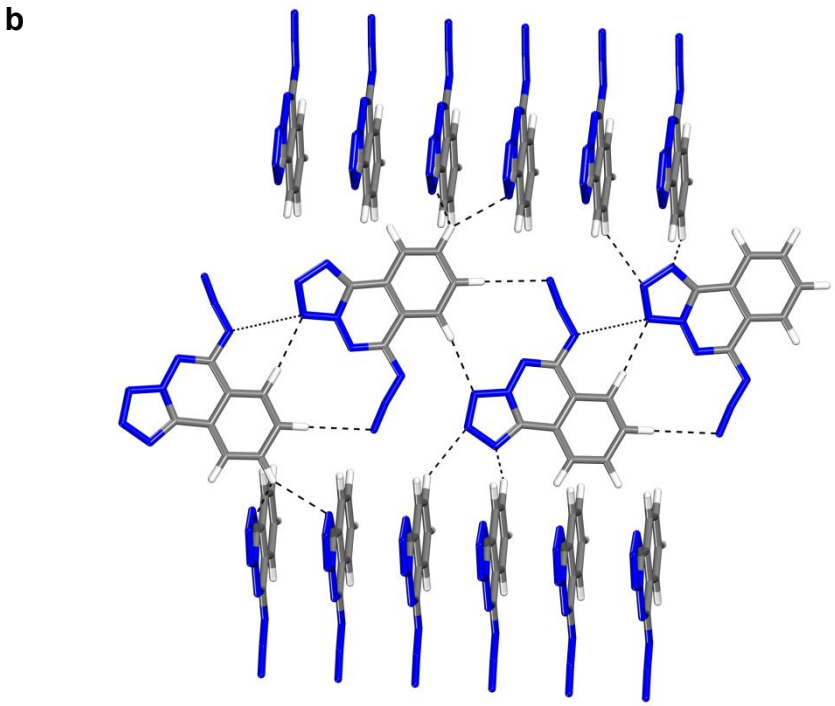

Figure 14. (a) Overlay of two predicted crystal structures of ATPH that have been re-optimized by periodic DFT-D. The structure shown in pink wireframe corresponds to observed Form I, and the structure shown with atoms in standard colors is that of the undiscovered low-energy $P2_12_12_1$ analogue. (b) Predicted crystal structure of the unobserved low-energy $Pca2_1$ polymorph of ATPH after periodic DFT-D re-optimization. The image shows the herringbone packing of tapes, with short N···N and N···H contacts indicated by broken lines.

Conclusions

ATPH is a nitrogen-rich compound of broad interest. It is purported to be a natural product, yet is closely related to substances developed as energetic materials and is highly polymorphic despite having a nearly planar structure with little flexibility. Routine screening has yielded seven solid

forms of ATPH, all characterized by single-crystal X-ray diffraction. The structures show diverse patterns of molecular organization, including both stacked sheets and herringbone packing. In all cases, N···N and C–H···N interactions play key roles in ensuring molecular cohesion. The high polymorphism of ATPH can be attributed in part to the ability of virtually every atom of nitrogen and hydrogen in the molecule to take part in close N···N and C–H···N contacts. As a result, adjacent molecules can be positioned in many different ways that are similar in energy, thereby giving rise to a polymorphic landscape with an unusually high density of potential structures. These conclusions are fully consistent with the results of in-depth computational studies. Knowledge gained by studying ATPH will be useful in the field of energetic materials, where access to multiple polymorphs can be used to clarify how performance depends on molecular packing. In addition, the behavior of ATPH confirms that broad insights about molecular crystallization, often acquired by subjecting structural databases to statistical analyses, can also come from using empirical and theoretical methods to study individual compounds that show distinctive behavior.

Experimental and Computational Methods

Computational Methodology Used in Gas-Phase Studies of ATPH. DFT calculations related to the isomerization of ATPH and its IR and Raman spectra used the B3LYP functional implemented in Gaussian 16,[66] as described in detail in the Supporting Information.

Initial Crystal Structure Prediction (CSP). CSP was performed using the Global Lattice Energy Explorer (GLEE) program.[67] GLEE uses a low-discrepancy, quasi-random sampling of crystal

packing variables to produce a uniform sampling of the lattice-energy surface. The gas-phase molecular structure of ATPH was first optimized in Gaussian 09 using PBE0/aug-cc-pVDZ with GD3BJ empirical dispersion.[68] The molecular structure was kept rigid throughout the initial CSP process. Trial structures were generated, and their lattice energies were minimized until 250,000 structures were obtained with one molecule in the asymmetric unit cell ($Z' = 1$). These structures were produced by sampling in the 25 most frequently observed space groups ($P2_1/c$, $P2_12_12_1$, $P\bar{1}$, $P2_1$, *Pbca*, $C2/c$, $Pna2_1$, *Cc*, $Pca2_1$, $C2$, $P1$, *Pbcn*, *Pc*, $P2_12_12$, *Fdd*2, *Pccn*, $P2/c$, $I4_1/a$, $R\bar{3}$, $P4_1$, $P4_32_12$, $P4_12_12$, $P4_3$, $P3_2$, and $P3_1$). 50,000 structures were generated in space groups $P2_1$ and $P2_1/c$, and 10,000 structures were produced in the other 23 space groups. A total of 100,000 structures were obtained with two molecules in the asymmetric unit cell ($Z' = 2$). These structures were produced by sampling the five most frequently observed space groups for $Z' = 2$ ($P\bar{1}$, $P2_1/c$, $P2_1$, $P2_12_12_1$, and $P1$). 10,000 structures were generated in $P1$, $P2_12_12_1$, and $P\bar{1}$, along with 20,000 in $P2_1$ and 50,000 in $P2_1/c$. Duplicates were removed from the resulting set of structures, initially within each space group by calculating the similarity of simulated powder X-ray diffraction patterns. Subsequently, more accurate removal of duplicates was carried out by using the COMPACK algorithm[63] for all structures within 2.39006 kcal mol^{-1} of the global minimum, irrespective of the space group of each structure. DMACRYS was used with an anisotropic atom-atom force-field energy model for all minimizations of lattice energy.[69] Lattice energies were calculated using the FIT forcefield[70] combined with molecular charge densities calculated from a Distributed Multipole Analysis (DMA)[71] of the MP2/aug-cc-pVDZ density with multipoles up to hexadecapole on each atom. The Polarizable Continuum Model (PCM) was applied to DMA to further improve the electrostatic model.

Re-optimization of Predicted Crystal Structures by Periodic DFT-D. All structures within a window of 1.195 kcal mol^{-1} were optimized using plane-wave-based periodic DFT as implemented in the VASP package.[64,65] Any matches to experimental structures that were not in the 1.195 kcal mol^{-1} window were also optimized. This optimization was done by a three-step procedure that has been noted to improve the convergence rate of periodic DFT optimizations for crystal structures.[72] The first step involves optimizing only the atomic positions, the second step optimizes both atomic positions and unit-cell parameters, and the third step is a final single-point calculation, so that the correct final energy is obtained. All VASP calculations were performed using the PBE exchange correlation function with Becke-Johnson-damped Grimme dispersion corrections. Projector augmented wave (PAW) potentials were used for all VASP calculations with the standard supplied pseudopotentials.

Experimental Methodology. All starting materials were purchased from commercial suppliers and used without further purification. Raman spectra were recorded with a Renishaw inVia Reflex spectrometer, using a 785 nm laser passing through an 1800 cm^{-1} grating and a 50× objective lens. DSC data were obtained by using a PerkinElmer DSC 6000 calorimeter with manually compressed Al pans containing samples weighing approximately 2 mg. Infrared spectra were recorded on a Bruker Alpha-P ATR FTIR spectrometer with 8 scans and a resolution of 4 cm^{-1}. Details related to X-ray diffraction using single crystals and powders are provided in the Supporting Information.

WARNING: Although no explosions involving ATPH occurred during our work, the compound decomposes vigorously when heated, with the evolution of copious volumes of black smoke. No more than about 5 g was ever prepared at one time, and precautions normally used in handling

potentially explosive materials were taken whenever ATPH was manipulated in solid form. It is important to note that closely related compounds have been reported to become more explosive as their purity and the size of their crystals increase.[30]

6-Azidotetrazolo[5,1-*a*]phthalazine (ATPH; 2). ATPH was synthesized as described by Reynolds et al.[12] To a stirred mixture of 1,4-dihydralazine (**5**; 4.00 g, 21.0 mmol) in water (35 mL), concentrated aqueous HCl (4 mL) and acetic acid (8 mL) were added. The mixture was then cooled in an ice bath, and a solution of $NaNO_2$ (4.0 g, 58 mmol) in water (20 mL) was added slowly at a rate that kept the temperature in the range 10–30 °C. The resulting brown solid was isolated by filtration and recrystallized from aqueous EtOH (95%) to obtain ATPH (**2**; 2.19 g, 10.3 mmol, 49%) as brown needles. Further purification was achieved by flash chromatography on silica gel (2:3 EtOAc:hexane gradient), which provided the compound as a pale yellow solid. The ^{1}H and ^{13}C NMR spectra matched those reported previously.[7]

Preparation of Essentially Phase-Pure Polymorphs of ATPH

Form I.[7] ATPH (50 mg) was dissolved in hot isopropanol (20 mL), and the solution was allowed to cool slowly to 25 °C and was then kept at 4 °C. Yield: 60%.

Form II. Crystals of Form I were cooled to 100 K.

Form III. ATPH (10 mg) was dissolved in a 1:1 mixture of acetone and isopropanol (1.0 mL), and the solvents were allowed to evaporate slowly at 25 °C. Yield: essentially quantitative.

Form IV. ATPH (10 mg) was dissolved in EtOAc (1.0 mL), and the solvent was allowed to evaporate on a hot plate at 50 °C. Yield: essentially quantitative.

Form V. ATPH (27 mg) was dissolved in $CHCl_3$ (1.0 mL), the solution was placed in a 4-mL vial, and the vial was put inside a 20-mL vial containing a small amount of hexane. The larger vial was closed, and vapors of hexane were allowed to diffuse into the solution in the smaller vial. Yield: 92%.

Form VI. Samples of solid ATPH were melted on a hot stage and kept at 160 °C for 2 min. Heating was stopped, and the stage was allowed to cool slowly to 25 °C. In random samples, Form VI appeared concomitantly with other polymorphs.

Form VII. ATPH (10 mg) was dissolved in a 1:1 mixture of 2-butanone and toluene (1.0 mL), and the solvents were allowed to evaporate slowly on a hot plate at 50 °C. Yield: essentially quantitative.

Notes. The authors have no competing financial interests to declare.

Supporting Information Available: Additional crystallographic details, descriptions of computational methods, and various experimental data, including spectroscopic characterizations, summaries of polymorphic screening, and analyses of solubility. This material is available free of charge via the Internet at http://pubs.acs.org.

Accession Codes. CCDC 2149764–2149772 contain the supplementary crystallographic data for this paper. These data can be obtained free of charge via www.ccdc.cam.ac.uk/data_request/cif, by emailing data_request@ccdc.cam.ac.uk, or by contacting The Cambridge Crystallographic Data Centre, 12 Union Road, Cambridge CB2 1EZ, UK; fax: +44 1223 336033.

Acknowledgments. Financial support from the Natural Sciences and Engineering Research Council (NSERC) of Canada (RGPIN-2019-05469) is gratefully acknowledged by J. D. W. In addition, J. D. W. thanks the Canada Foundation for Innovation (Project 30910), the Canada Research Chairs Program, and the Université de Montréal for their generous support. J. E. A. and G. M. D. thank the Air Force Office of Scientific Research for funding under Award No. FA8655-20-1-7000. Through membership in the HEC Materials Chemistry Consortium, which is funded by the Engineering and Physical Sciences Research Council (EPSRC) of the United Kingdom via grant EP/R029431, we used computational resources provided by the Materials and Molecular Modelling Hub (MMM Hub), which is partially funded by EPSRC (EP/T022213). In addition, we are grateful to Dr. Michel Simard for early crystallographic investigations, Dr. Pedro M. Aguiar for his assistance in obtaining variable-temperature NMR spectra, and Dr. Samir Elouatik for helping us record Raman spectra.

References

1. Wibowo, M.; Ding, L. Chemistry and Biology of Natural Azoxy Compounds. *J. Nat. Prod.* **2020**, *83*, 3482–3491.
2. Le Goff, G.; Ouazzani, J. Natural Hydrazine-Containing Compounds: Biosynthesis, Isolation, Biological Activities and Synthesis. *Bioorg. Med. Chem.* **2014**, *22*, 6529–6544.
3. Blair, L. M.; Sperry, J. Natural Products Containing a Nitrogen–Nitrogen Bond. *J. Nat. Prod*. **2013**, *76*, 794–812.
4. Nawrat, C. C.; Moody, C. J. Natural Products Containing a Diazo Group. *Nat. Prod. Rep*. **2011**, *28*, 1426–1444.

5. LaRue, T. A. Naturally Occurring Compounds Containing a Nitrogen–Nitrogen Bond. *Lloydia* **1977**, *76*, 307–321.

6. Langley, B. W.; Lythgoe, B.; Riggs, N. V. Macrozamin. Part II. The Aliphatic Azoxy Structure of the Aglycone Part. *J. Chem. Soc*. **1951**, 2309–2316.

7. Hossain, M. B.; van der Helm, D.; Sanduja, R.; Alam, M. Structure of 6-Azidotetrazolo[5,l-*a*]phthalazine, $C_8H_4N_8$, Isolated from the Toxic Dinoflaggelate *Gymnodinium breve*. *Acta Crystallogr.* **1985**, *C41*, 1199−1202.

8. Elsharabasy, F. S.; Gomha, S. M.; Farghaly, T. A.; Elzahabi, H. S. A. An Efficient Synthesis of Novel Bioactive Thiazolyl-Phthalazinediones under Ultrasound Irradiation. *Molecules* **2017**, *22*, 319.

9. Winter, J. M.; Jansma, A. L.; Handel, T. M.; Moore, B. S. Formation of the Pyridazine Natural Product Azamerone by Biosynthetic Rearrangement of an Aryl Diazoketone. *Angew. Chem. Int. Ed.* **2009**, *48*, 767–770.

10. Cho, J. Y.; Kwon, H. C.; Williams, P. G.; Jensen, P. R.; Fenical, W. Azamerone, a Terpenoid Phthalazinone from a Marine-Derived Bacterium Related to the Genus *Streptomyces* (Actinomycetales). *Org. Lett.* **2006**, *8*, 2471–2474.

11. Stollé, R.; Storch, H. Über de Umsetzung von Dichlor-1,4-phtalazin mit Natriumazid. *J. Prakt. Chem.* **1932**, *135*, 128–136.

12. Reynolds, G. A.; VanAllan, J. A.; Tinker, J. F. Cyclization of Certain Heterocyclic Azides. *J. Org. Chem.* **1959**, *24*, 1205−1209.

13. Tišler, M. Some Aspects of Azido–Tetrazolo Isomerization. *Synthesis* **1973**, 123–136.

14. Krivopalov, V. P.; Baram, S. G.; Denisov, A. Yu.; Mamatyuk, V. I. Azide-Tetrazole Tautomerism of Diazidodiazines and Their Benzo Analogs. *Izv. Akad. Nauk SSSR, Ser. Khim.* **1989**, 2002−2007.

15. Katsuyama, Y.; Matsuda, K. Recent Advance in the Biosynthesis of Nitrogen–Nitrogen Bond–Containing Natural Products. *Curr. Opin. Chem. Biol*. **2020**, *59*, 62–68.

16. Guo, Y.-Y.; Li, Z.-H.; Xia, T.-Y.; Du, Y.-L.; Mao, X.-M.; Li, Y.-Q. Molecular Mechanisms of Azoxy Bond Formation for Azoxymycins Biosynthesis. *Nat. Commun.* **2019**, 10, 4420.

17. Waldman, A. J.; Ng, T. L.; Wang, P.; Balskus, E. P. Heteroatom−Heteroatom Bond Formation in Natural Product Biosynthesis. *Chem. Rev.* **2017**, *117*, 5784–5863.

18. Matsuda, K.; Tomita, T.; Shin-ya, K.; Wakimoto, T.; Kuzuyama, T.; Nishiyama, M. Discovery of Unprecedented Hydrazine-Forming Machinery in Bacteria. *J. Am. Chem. Soc.* **2018**, *140*, 9083–9086.

19. Sugai, Y.; Katsuyama, Y.; Ohnishi, Y. A Nitrous Acid Biosynthetic Pathway for Diazo Group Formation in Bacteria. *Nat. Chem. Biol.* **2016**, *12*, 73–75.

20. Badgujar, D. M.; Talawar, M. B.; Asthana, S. N.; Mahulikar, P. P. Advances in Science and Technology of Modern Energetic Materials: An Overview. *J. Hazard. Mater.* **2008**, *151*, 289−305.

21. Waller, A. R.; Chasseaud, L. F.; Taylor, T. Structure of the Product of Reaction Between Dihydralazine and Nitrous Acid. *J. Chromatogr.* **1979**, *179*, 392−393.

22. Huang, W.; Tang, Y.; Imler, G. H.; Parrish, D. A.; Shreeve, J. M. Nitrogen-Rich Tetrazolo[1,5-*b*]pyridazine: Promising Building Block for Advanced Energetic Materials. *J. Am. Chem. Soc.* **2020**, *142*, 3652–3657.

23. Chen, S.; Liu, Y.; Feng, Y.; Yang, X.; Zhang, Q. 5,6-Fused Bicyclic Tetrazolo-Pyridazine Energetic Materials. *Chem. Commun.* **2020**, *56*, 1493–1496.
24. Bernstein, J. *Polymorphism in Molecular Crystals*; Oxford University Press: New York, 2002.
25. Kersten, K.; Kaur, R.; Matzger, A. Survey and Analysis of Crystal Polymorphism in Organic Structures. *IUCrJ* **2018**, *5*, 124−129.
26. López-Mejías, V.; Kampf, J. W.; Matzger, A. J. Nonamorphism in Flufenamic Acid and a New Record for a Polymorphic Structure with Solved Structures. *J. Am. Chem. Soc.* **2012**, *134*, 9872−9875.
27. Yu, L. Polymorphism in Molecular Solids: An Extraordinary System of Red, Orange, and Yellow Crystals. *Acc. Chem. Res*. **2010**, *43*, 1257−1266.
28. Lévesque, A.; Maris, T.; Wuest, J. D. ROY Reclaims Its Crown: New Ways To Increase Polymorphic Diversity. *J. Am. Chem. Soc.* **2020**, *142*, 11873−11883.
29. Tyler, A. R.; Ragbirsingh, R.; McMonagle, C. J.; Waddell, P. G.; Heaps, S. E.; Steed, J. W.; Thaw, P.; Hall, M. J.; Probert, M. R. Encapsulated Nanodroplet Crystallization of Organic-Soluble Small Molecules. *Chem* **2020**, *6*, 1–11.
30. Keßenich, E.; Klapötke, T. M.; Knizek, J.; Nöth, H.; Schulz, A. Characterization, Crystal Structure of 2,4-Bis(triphenylphosphanimino)tetrazolo[5,1-*a*]-[1,3,5]triazine, and Improved Crystal Structure of 2,4,6-Triazido-1,3,5-triazine. *Eur. J. Inorg. Chem.* **1998**, 2013–2016.
31. Jack, D. B. Measurement of Dihydralazine by High-Performance Liquid Chromatography. *J. Chromatogr.* **1979**, *179*, 390−391.
32. Waller, A. R.; Chasseaud, L. F.; Taylor, T. High-Performance Liquid Chromatographic Determination of Dihydralazine in Human Plasma. *J. Chromatogr.* **1979**, *179*, 202−207.

33. Klapötke, T. M.; Krumm, B.; Martin, F. A.; Stierstorfer, J. New Azidotetrazoles: Structurally Interesting and Extremely Sensitive. *Chem. Asian J.* **2012**, *7*, 214−224.

34. Murray, J. S.; Concha, M. C.; Politzer, P. Links Between Surface Electrostatic Potentials of Energetic Molecules, Impact Sensitivities and C–NO_2/N–NO_2 Bond Dissociation Energies. *Mol. Phys.* **2009**, *107*, 89–97.

35. Zeman, S. Sensitivities of High Energy Compounds. *Struct. Bond.* **2007**, *125*, 195–271.

36. Olejniczak, A.; Katrusiak, A.; Podsiadło, M.; Katrusiak, A. Crystal Design by CH···N and N···N Interactions: High-Pressure Structures of High-Nitrogen-Content Azido-Triazolopyridazines Compounds. *Acta Crystallogr.* **2020**, *B76*, 1136–1142.

37. Olejniczak, A.; Katrusiak, A.; Podsiadło, M.; Katrusiak, A. Short N···N and CH···N Contacts in the Ambient and High-Pressure Polymorphs of a High Nitrogen-Content Compound. *Cryst. Growth Des.* **2019**, *19*, 1832–1838.

38. Stierstorfer, J.; Klapötke, T. M.; Hammerl, A.; Chapman, R. D. 5-Azido-1*H*-tetrazole — Improved Synthesis, Crystal Structure and Sensitivity Data. *Z. Anorg. Allg. Chem*. **2008**, *634*, 1051−1057.

39. Golič, L.; Leban, I.; Stanovnik, B.; Tišler, M. The Crystal Structures of *s*-Triazolo[4,3-*b*]pyridazine, *s*-Triazolo[1,5-*b*]pyridazine and Tetrazolo[l,5-*b*]pyridazine. *Acta Crystallogr.* **1978**, *B34*, 1136−1140.

40. Müller, U. Strukturchemie der Azide. *Struct. Bond.* **1973**, *14*, 141−172.

41. Bräse, S.; Gil, C.; Knepper, K.; Zimmermann, V. Organic Azides: An Exploding Diversity of a Unique Class of Compounds. *Angew. Chem. Int. Ed.* **2005**, *44*, 5188−5240.

42. Athiyarath, V.; Sureshan, K. M. Designed Synthesis of a 1D Polymer in Twist-Stacked Topology via Single-Crystal-to-Single-Crystal Polymerization. *Angew. Chem. Int. Ed.* **2020**, *59*, 15580−15585.

43. Shields, D. J.; Karothu, D. P.; Sambath, K.; Ranaweera, R. A. A. U.; Schramm, S.; Duncan, A.; Duncan, B.; Krause, J. A.; Gudmundsdottir, A. D.; Naumov, P. Cracking under Internal Pressure: Photodynamic Behavior of Vinyl Azide Crystals through N_2 Release. *J. Am. Chem. Soc.* **2020**, *142*, 18565−18575.

44. Bursch, M.; Kunze, L.; Vibhute, A. M.; Hansen, A.; Sureshan, K. M.; Jones, P. G.; Grimme, S.; Werz, D. B. Quantification of Noncovalent Interactions in Azide–Pnictogen, –Chalcogen, and –Halogen Contacts. *Chem. Eur. J.* **2020**, 27, 4627−4639.

45. Baxter, A. F.; Martin, I.; Christe, K. O.; Haiges, R. Formamidinium Nitroformate: An Insensitive RDX Alternative. *J. Am. Chem. Soc.* **2018**, *140*, 15089−15098.

46. Wang, Q.; Shao, Y.; Lu, M. $C_8N_{12}O_8$: A Promising Insensitive High-Energy-Density Material. *Cryst. Growth Des.* **2018**, *18*, 6150−6154.

47. Zhang, J.; Mitchell, L. A.; Parrish, D. A.; Shreeve, J. M. Enforced Layer-by-Layer Stacking of Energetic Salts towards High-Performance Energetic Materials. *J. Am. Chem. Soc.* **2015**, *137*, 10532−10535.

48. Zhang, C.; Wang, X.; Huang, H. π-Stacked Interactions in Explosive Crystals: Buffers against External Mechanical Stimuli. *J. Am. Chem. Soc.* **2008**, *130*, 8359−8365.

49. For additional details, see the Supporting Information.

50. Michalchuk, A. A. L.; Rudić, S.; Pulham, C. R.; Morrison, C. A. Predicting the Impact Sensitivity of a Polymorphic High Explosive: The Curious Case of FOX-7. *Chem. Commun.* **2021**, *57*, 11213−11216.

51. Miller, G. R.; Garroway, A. N. *A Review of the Crystal Structures of Common Explosives Part I: RDX, HMX, TNT, PETN, and Tetryl*; Report NRL/MR/6120--01-8585; Naval Research Laboratory: Washington, DC, 2001.

52. Nyman, J.; Day, G. M. Static and Lattice Vibrational Energy Differences Between Polymorphs. *CrystEngComm* **2015**, *17*, 5154−5165.

53. McCrone, W. C. In *Polymorphism in Physics and Chemistry of the Organic Solid State*; Fox, D.; Labes, M. M.; Weissenberg, A., Eds.; Interscience: New York, 1965, Vol. II, pp 725–767.

54. Brás, E. M.; Henriques, M. S. C.; Paixão, J. A.; Fausto, R. High Z' Crystal Structure of a New Polymorph of a Thioimidazole Disulfide: Importance of Conformational Flexibility. *Cryst. Growth Des.* **2018**, *18*, 4167−4173.

55. Cruz-Cabeza, A. J.; Reutzel-Edens, S. M.; Bernstein, J. Facts and Fictions about Polymorphism. *Chem. Soc. Rev.* **2015**, *44*, 8619−8635.

56. Hirshfeld surfaces and two-dimensional fingerprint plots were generated by using CrystalExplorer17. Turner, M. J.; McKinnon, J. J.; Wolff, S. K.; Grimwood, D. J.; Spackman, P. R.; Jayatilaka, D.; Spackman, M. A. *CrystalExplorer17*; University of Western Australia, 2017.

57. McKinnon, J. J.; Spackman, M. A.; Mitchell, A. S. Novel Tools for Visualizing and Exploring Intermolecular Interactions in Molecular Crystals. *Acta Crystallogr. B* **2004**, *60*, 627–668.

58. Heskia, A.; Maris, T.; Wuest, J. D. Phosphangulene: A Molecule for All Chemists. *Acc. Chem. Res.* **2020**, *53*, 2472–2482.

59. Heskia, A.; Maris, T.; Wuest, J. D. Foiling Normal Patterns of Crystallization by Design. Polymorphism of Phosphangulene Chalcogenides. *Cryst. Growth Des.* **2019**, *19*, 5390–5406.

60. Day, G. M. Current Approaches to Predicting Molecular Organic Crystal Structures. *Crystallogr. Rev.* **2011**, *17*, 3–52.

61. Price, S. L.; Leslie, M.; Welch, G. W. A.; Habgood, M.; Price, L. S.; Karamertzanis, P. G.; Day, G. M. Modelling Organic Crystal Structures Using Distributed Multipole and Polarizability-Based Model Intermolecular Potentials. *Phys. Chem. Chem. Phys.* **2010**, *12*, 8478–8490.

62. Coombes, D. S.; Price, S. L.; Willock, D. J.; Leslie, M. Role of Electrostatic Interactions in Determining the Crystal Structures of Polar Organic Molecules. A Distributed Multipole Study. *J. Phys. Chem.* **1996**, *100*, 7352–7360.

63. Chisholm, J. A.; Motherwell, S. *COMPACK*: A Program for Identifying Structure Similarity Using Distances. *J. Appl. Cryst.* **2005**, *38*, 228–231.

64. Kresse, G.; Furthmüller, J. Efficient Iterative Schemes for *Ab Initio* Total-Energy Calculations Using a Plane-Wave Basis Set. *Phys. Rev. B* **1996**, *54*, 11169–11186.

65. Kresse, G.; Furthmüller, J. Efficiency of Ab-Initio Total Energy Calculations for Metals and Semiconductors Using a Plane-Wave Basis Set. *Comput. Mater. Sci.* **1996**, *6*, 15–50.

66. Frisch, M. J.; Trucks, G. W.; Schlegel, H. B.; Scuseria, G. E.; Robb, M. A.; Cheeseman, J. R.; Scalmani, G.; Barone, V.; Petersson, G. A.; Nakatsuji, H.; Li, X.; Caricato, M.; Marenich, A. V.; Bloino, J.; Janesko, B. G.; Gomperts, R.; Mennucci, B.; Hratchian, H. P.; Ortiz, J. V.; Izmaylov, A. F.; Sonnenberg, J. L.; Williams; Ding, F.; Lipparini, F.; Egidi, F.; Goings, J.; Peng, B.; Petrone, A.; Henderson, T.; Ranasinghe, D.; Zakrzewski, V. G.; Gao, J.; Rega, N.; Zheng, G.; Liang, W.; Hada, M.; Ehara, M.; Toyota, K.; Fukuda, R.; Hasegawa, J.; Ishida, M.; Nakajima, T.; Honda, Y.; Kitao, O.; Nakai, H.; Vreven, T.; Throssell, K.; Montgomery Jr., J. A.; Peralta, J. E.; Ogliaro, F.; Bearpark, M. J.; Heyd, J. J.; Brothers, E. N.; Kudin, K. N.;

Staroverov, V. N.; Keith, T. A.; Kobayashi, R.; Normand, J.; Raghavachari, K.; Rendell, A. P.; Burant, J. C.; Iyengar, S. S.; Tomasi, J.; Cossi, M.; Millam, J. M.; Klene, M.; Adamo, C.; Cammi, R.; Ochterski, J. W.; Martin, R. L.; Morokuma, K.; Farkas, O.; Foresman, J. B.; Fox, D. J. *Gaussian 16, Revision C.01*. Gaussian, Inc., Wallingford, CT, 2016.

67. Case, D. H.; Campbell, J. E.; Bygrave, P. J.; Day, G. M. Convergence Properties of Crystal Structure Prediction by Quasi-Random Sampling. *J. Chem. Theory Comput.* **2016**, *12*, 910–924.

68. Frisch, M. J.; Trucks, G. W.; Schlegel, H. B.; Scuseria, G. E.; Robb, M. A.; Cheeseman, J. R.; Scalmani, G.; Barone, V.; Petersson, G. A.; Nakatsuji, H.; Li, X.; Caricato, M.; Marenich, A.; Bloino, J.; Janesko, B. G.; Gomperts, R.; Mennucci, B.; Hratchian, H. P.; Ortiz, J. V.; Izmaylov, A. F.; Sonnenberg, J. L.; Williams-Young, D.; Ding, F.; Lipparini, F.; Egidi, F.; Goings, J.; Peng, B.; Petrone, A.; Henderson, T.; Ranasinghe, D.; Zakrzewski, V. G.; Gao, J.; Rega, N.; Zheng, G.; Liang, W.; Hada, M.; Ehara, M.; Toyota, K.; Fukuda, R.; Hasegawa, J.; Ishida, M.; Nakajima, T.; Honda, Y.; Kitao, O.; Nakai, H.; Vreven, T.; Throssell, K.; Montgomery, J. A., Jr.; Peralta, J. E.; Ogliaro, F.; Bearpark, M.; Heyd, J. J.; Brothers, E.; Kudin, K. N.; Staroverov, V. N.; Keith, T.; Kobayashi, R.; Normand, J.; Raghavachari, K.; Rendell, A.; Burant, J. C.; Iyengar, S. S.; Tomasi, J.; Cossi, M.; Millam, J. M.; Klene, M.; Adamo, C.; Cammi, R.; Ochterski, J. W.; Martin, R. L.; Morokuma, K.; Farkas, O.; Foresman, J. B.; Fox, D. J. *Gaussian 09, Revision A.02.* Gaussian, Inc., Wallingford CT, 2016.

69. Price, S. L.; Leslie, M.; Welch, G. W. A.; Habgood, M.; Price, L. S.; Karamertzanis, P. G.; Day, G. M. Modelling Organic Crystal Structures Using Distributed Multipole and Polarizability-Based Model Intermolecular Potentials. *Phys. Chem. Chem. Phys.* **2010**, *12*, 8478–8490.

70. Coombes, D. S.; Price, S. L.; Willock, D. J.; Leslie, M. Role of Electrostatic Interactions in Determining the Crystal Structures of Polar Organic Molecules. A Distributed Multipole Study. *J. Phys. Chem.* **1996**, *100*, 7352–7360.

71. Stone, A. J.; Alderton, M. Distributed Multipole Analysis. Methods and Applications. *Mol. Phys.* **2002**, *100*, 221–233.

72. Taylor, C. R.; Day, G. M. Evaluating the Energetic Driving Force for Cocrystal Formation. *Cryst. Growth Des.* **2018**, *18*, 892–904.